Tubular Self-Piercing Riveting Applied to Butt Joints

Leonardo Lúcio de Melo Sabino

Thesis to obtain the Master of Science Degree in

Mechanical Engineering

Supervisors: Prof. Luís Manuel Mendonça Alves

Prof. Rafael Augusto Nunes Miranda Malta Afonso

Examination Committee

Chairperson: Prof. Rui Manuel dos Santos Oliveira Baptista

Supervisor: Prof. Luís Manuel Mendonça Alves

Members of the Committee: Prof. Virgínia Isabel Monteiro Nabais Infante

Prof. Catarina Isabel Silva Vidal

November 2023

Declaration

I declare that this document is an original work of my authorship and that it fulfils all the requirements of the Code of Conduct and Good Practices of the Universidade de Lisboa.

Resumo

A rebitagem auto-perfurante (SPR) é um processo de deformação plástica a frio utilizado para unir chapas de materiais metálicos, poliméricos ou compósitos. É um processo frequentemente utilizado na indústria automóvel, por exemplo. Consiste em inserir um rebite nas chapas a ligar numa única operação, sem estas serem pré-furadas, criando uma ligação permanente e económica. A indústria automóvel é pressionada a produzir veículos mais eficientes e leves para responder a normas cada vez mais apertadas de emissões de gases de escape para novos veículos de combustão interna e para produzir veículos elétricos com maior autonomia. Com efeito, novos materiais foram introduzidos no fabrico de componentes estruturais desses veículos, como ligas de alumínio e magnésio, entre outros, substituindo ligas de aço. Para alguns dos materiais, os processo, como a soldadura por pontos, não são competitivos ou até aplicáveis. Uma solução que tem vindo a crescer significativamente em uso é a rebitagem auto-perfurante (SPR). Normalmente, as superfícies dos materiais são estendidas, perfazendo uma junta sobreposta, o que implica mais material e peso. Este trabalho procura responder à questão de se um processo de SPR poderá ser implementado em juntas topo-a-topo, apresentando uma análise de exequibilidade da variante tubular-SPR aplicada a juntas topo-a-topo, sem chapas auxiliares e utilizando ferramentas planas. É dado ênfase a ligações entre chapas de alumínio, mas também foram ligadas chapas de cobre e policloreto de vinila (PVC). Verificou-se ser possível unir chapas, com $\mathbf{5}\boldsymbol{mm}$ de espessura, topo-a-topo, sendo que rebites mais finos e mais altos produzem as ligações mais resistentes.

Palavras-chave: Rebitagem auto-perfurante tubular, Ligações topo-a-topo, Rebitagem auto-perfurante, Curva força-deslocamento

Abstract

Self-piercing riveting (SPR) is a cold-forming process widely used to join sheets of whether metallic, polymeric or composite materials. It is a process regularly found in the automotive industry, for instance. It consists of inserting a rivet into the workpiece in a single-stroke operation, without any pre-drilled holes, creating a permanent and cost-effective connection. Automakers have been pushed into producing vehicles that are more efficient and lighter to respond to ever tighter emissions standards for new internal combustion engine vehicles on the market, and to produce longer-ranging electric vehicles. As a result, new materials have been introduced into vehicles' mass manufacturing, such as aluminium and magnesium alloys, among others, replacing heavier steel in structural components. For some of these materials the processes, such as resistance spot welding, are no longer competitive or even applicable. One manufacturing solution that had significant growth in use is Self-Piercing Riveting (SPR). Usually, the materials' surfaces are extended to overlap each other and perform a lap joint. This overlap means more weight. This work reports on the question if a SPR process could be implemented with butt joints, presenting a feasibility analysis of the Tubular-SPR variant applied to butt joints, without auxiliary straps and using flat tools. It is given emphasis to aluminium workpieces, but copper and polyvinyl chloride (PVC) workpieces were also tested. It was observed that it is possible to join sheets of $\mathbf{5}\boldsymbol{mm}$ thickness in such a configuration, with thinner and taller rivets producing connections with the most mechanical resistance.

Keywords: Tubular self-piercing riveting, Butt joint, Self-piercing riveting, Force-displacement curve

Acknowledgements

I would like to thank my supervisors Professor Luís Alves and Professor Rafael Afonso, with whom I have learned much, for their support, guidance and availability throughout this work.

I would like to show my deepest gratitude towards my parents, brother and aunt Mila, who so much effort have put through the years into making me a young man with a course and life experiences I could be proud of. I am very fortunate for having them to share the good and bad moments, and getting always the best advice.

A long due thank you to Maria Portijo for being a great partner through the whole time of developing this work, but mostly for all her patience and the help she has provided me through the course. I must thank her for persuading me into joining Técnico Solar Boat, which opened to me new horizons and prospects.

Contents

Declaration iii
Resumo v
Abstract vii
Acknowledgements ix
List of Tables xiii
List of Figures xv
List of Symbols xvii
Acronyms xix

1 Introduction **1**

1.1 Riveting overview 1
1.2 Motivation 2
1.3 Objectives and deliverables 3

2 State-of-the-art **4**

2.1 Introduction to SPR 4
2.2 Alternative technologies and brief comparison 8
2.3 SPR variants and solutions 11
2.4 Tubular self-piercing riveting 13
2.5 Rivet geometry 14

3 Methods **18**

3.1 Work overview 18
3.2 Rivets' fabrication 19
3.3 Joining materials and sheets' fabrication 20
3.4 Setups 21
3.4.1 Riveting setup 22
3.4.2 Tensile-shear setup 23
3.4.3 Three-point bending setup 24
3.5 Data processing 25
3.5.1 Compensation of the force-displacement curves 25
3.5.2 Extraction and calculation of the results 26

4 Experimental results **29**

4.1 Riveting setup and curves analysis 29
4.2 Variation of rivet thickness 33
4.3 Variation of rivet height 38

4.4 Workpiece's material joinability 43
4.5 Riveting method for improved mechanical resistance 45
5 Conclusions **49**
5.1 Achievements and conclusions 49
5.2 Future work 51
Bibliography **53**

List of Tables

1 Mechanical properties of the sheets' materials. 21

2 Riveting parameters for the setup tests. 30

3 Riveting results of the setup tests. 31

4 Riveting results of the rivet thickness tests. 34

5 Tensile-shear tests' results and mechanical interlocking of joints with different rivet thicknesses 35

6 Three-point bending tests' results. 37

7 Riveting results of the rivet height tests. 39

8 Tensile-shear tests' results of connections with different height rivets. 41

9 Riveting tests' results of different workpiece materials combinations 43

10 Results of riveting the double riveted connection. 47

11 Tensile-shear tests' results of the connection with two standard rivets, single standard rivet and single $h = 7mm$ rivet 47

List of Figures

1 Section view of a butt joint between two aluminium sheets using T-SPR technology.....3

2 Illustration of the cross-section of a SPR connection, depicted with the rivet's head height, h_h, undercut, u, and remaining bottom thickness, t_b. Adapted from [8]. 6

3 A force–displacement curve of a SPR process [10]. 7

4 Illustration of the process stages in flow drill screw driving: (a) heating, penetration, and bush forming; (b) thread forming and screw advancing; (c) tightening [11]. 8

5 Process of the single-point butt clinching [15]. 9

6 Illustration of the electrical resistances in a sheet stack-up during RSW [17].....9

7 Section view of the T-SPR rivet and its dimensional parameters. 14

8 Flange-type tubular rivets.....15

9 DSSPR process window for rivets with 10mm external diameter and 45º chamfer angle, in joints of similar thickness sheets [32]. 15

10 Assumption of equivalence between T-SPR in a butt joint, at the left, and conventional DSSPR, at the right. 16

11 Dimensions on the section view of this study's standard rivet. 16

12 Study overview. 19

13 Manufacturing of the rivets.....20

14 Riveting setup: at the left is the machine and plattens; at the right is a close-up view of the steel support with two aluminium sheets and the rivet positioned. 23

15 Close-up view of the flexural tests' setup.....24

16 Riveting curve with rivet's setting point. 26

17 Measured features for interlock calculation. 27

18 Illustration of the points used for the gap measurement.....28

19 Riveting curves of the setup tests.....31

20 Riveted sheets with iteration I, II and III of the setup from top to bottom, respectively. 32

21 Riveting curves of the rivet’s thickness tests.....33

22 Tensile-shear tests' curves of joints with different rivet thicknesses.. 34

23 Tensile-shear test with the unfastening mechanism between the rivet and the top sheet. 36

24 Illustration of the flexural tests’s direct orientation (DO), on the left, and inverse orientation (IO), on the right. 36

25 Three-point bending flexural tests’ curves. 37

26 Close-up view of the teared material from the joint under three-point bending flexural testing, in the DO orientation. 38

27 Riveting curves of the various rivet’s height tests. 39

28 Tensile-shear tests' curves of connections with different rivet heights.. 40

29 Destroyed joints after tensile-shear testing. Figure at the left, without signs of sheet tearing. Figure at the right with signs of tearing.....41

30 Non-dimensionalized tendencies of rivet height, interlock and maximum tensile load.....42

31 Riveting curves of the Al-Al, Al-Cu and Cu-Cu joints.....43
32 PVC-PVC joint, riveted with standard rivet. 44
33 Riveting curves of the PVC-PVC and Al-Al joints with $t = 1mm$ rivets.....45
34 Riveting curves of the double riveted connection.....46
35 Tensile-shear tests' curves of the connection with two standard rivets, single standard rivet and single $h = 7mm$ rivet.....47
36 Rivets attached to the top sheet after rupture of bottom sheet in double riveted conncetion...48

List of Symbols

α	tubular rivet's chamfer angle
β	angle of the rivet's deformation during tensile-shear testing
θ	chamfer angle of the flange-type rivet
c	rivet's tip width
C	trajectory for which work is calculated
d	rivet's external diameter
d_s	displacement of the rivet at the time it is set
D_h	rivet's head diameter after riveting
D_s	diameter of the rivet's flared skirt
E_{bend}	energy absorbed by the connection until failure under three-point bending flexural testing
E_{tens}	energy absorbed by the connection until failure under tensile-shear testing
F	scalar value of the force vector
$\vec{F}$	force vector
F_{bend}	maximum force supported by the connection in three-point bending flexural testing
F_{set}	force applied for rivet setting
F_{tens}	maximum force supported by the connection in tensile-shear testing
g	gap between the faying surfaces
G'	first place for the faying surfaces' gap measurement
G''	second place for the faying surfaces' gap measurement
h	rivet's height
h_{pierce}	rivet's height after piercing
i	interlock
M	maximum moment supported by the connection in three-point bending flexural testing
n	number of data points
r	scalar value of the displacement vector

$\vec{r}$	displacement vector
t	rivet's wall thickness
W_C	work along a trajectory C
W_{set}	work applied to the rivet until rivet setting

Acronyms

DO Direct orientation

DSSPR Double-sided self-piercing riveting

FDS Flow drill screwing

F-SPR Friction self-piercing riveting

IO Inverse orientation

LTM Laboratório de Tecnologia Mecânica

NDT Non-destructive testing

P-SPR Padded self-piercing riveting

PVC polyvinyl chloride

RSW Resistance spot welding

SPR Self-piercing riveting

SPTR Self-piercing-through riveting

T-SPR Tubular self-piercing riveting

Chapter 1

Introduction

1.1 - Riveting overview

During the industrial revolution, riveting with solid rivets was key, enabling the industrial and infrastructure boom of the time. Still today, there are many testimonies of this period, with the Eiffel Tower probably being the most well-known. However, rivets have been around for a very long time, as the earlier findings take riveting as far as around 3000B.C. in Egypt, used for joining a variety of objects and tools. Throughout history, riveting continued to have an important role among different peoples. The Roman empire and later the Viking communities are some of the peoples that widely used riveting techniques [1].

Cold riveting and hot riveting were the most used riveting processes. They consist of mechanically joining together either similar or dissimilar materials, in a permanent connection, using a fastener called the rivet. The rivet is shaped as a cylinder with a pre-manufactured hemispherical head. The process requires a predrilled hole in the joining materials, a punch and a counter punch. First, the materials are aligned by the predrilled hole. Then the rivet is inserted, with the counter punch holding the rivet's manufactured head while the punch plastically deforms the other end of the rivet, so that it cannot release itself, securing the materials together.

Over the years technology evolved and so did riveting. Many variants of the process have been invented, making riveting a more competitive and up-to-date technology. Self-piercing riveting (SPR) is one of the variants, with its roots in the second half of the 20th century. SPR has been gaining presence in the automotive industry since the 1990s with its introduction in the mass production of the Audi A8 [2]. In fact, the automotive industry has been the major propeller of SPR technology development. Manufacturers facing pressure to improve vehicles' efficiency and to meet emissions targets, see weight reduction as an important subject worth investing in. This caused a shift on the materials used in the body of the vehicles, from steels to aluminium alloys, high-strength and ultra-high-strength steel, and a wide range of composite materials. The mismatch of materials creates challenges to well-established joining technologies, such as resistance spot welding (RSW), and leads to the growth of different ones, such as SPR.

SPR consists of a riveting process in which the rivet is pressed into the sheets of material to join, without the need to pre-drill a hole. As the rivet is set, it pierces into the joining materials, creating a mechanical connection, hence the name self-piercing riveting. This technology stands out from conventional riveting, because it is a quick process, that reduces the number of assembly operations and allows less strict tolerances within assemblies as it is no longer required to pre-drill the joining materials to perform the connection. Unlike welding processes, riveting can join a wide range of materials, from metals to polymers and ceramics, in either similar or dissimilar material joints. Self-

piercing riveting can provide connections regardless of the surface finishing or films present on the materials, such as rugosity, paint, or anodization treatment due to its nature of mechanical locking. It also presents the advantage of not generating fumes or sparks and making low noise [2]. The surface quality insensitivity and the speed of the process also represent two main factors when considering SPR technology over adhesive bonding.

Tubular self-piercing riveting is identical to SPR, but it makes use of tubular rivets. In this study, the technology was used in butt joints without auxiliary straps. No dedicated dies were used, but rather flat tools, so that the rivet stays flush with the joining materials in both sides of the connection.

1.2 - Motivation

The industry is always refining processes and looking for technologies that allow joining materials in a simpler and cheaper way. Currently, there are many different joining processes, and these are generally classified into three major groups: adhesive bonding, welding and mechanical joining. Additionally, some joints might come as a result of the application of distinct technologies. Such cases are known as hybrid joining technologies, which aim to combine the advantages of various technologies in a single joint.

Regarding mechanical joining processes, there are many different types and variants. Some require additional fasteners such as screwing, or riveting. Others don't require any fastener at all, such as clinching or hemming. The work here presented focuses on a specific variant of riveting. Riveting is a group of permanent joining processes used to join sheets or plates of materials, using an additional element that is added to the connection, called the rivet. During the process, the rivet is plastically deformed, creating a mechanical lock that ensures the connection. Rivets can be found in a diversity of shapes and sizes to better suit each application. The many existing variants aim to provide certain attributes that other riveting types do not guarantee, such as a lower riveting load, joint impermeability, or flushness with the joining surfaces, among others.

Despite being an ancient technology, many improvements and variations still make riveting an up-to-date technology that is used in applications everywhere from the wings of aeroplanes to the structure of road vehicles, or from bridges to road signs, and in many other consumer goods.

The work here presented comes with the objective of broadening the range of applications of tubular self-piercing riveting (T-SPR) from overlapped to butt joint configurations using flat tools, instead of dedicated dies. If successful, this joining configuration could represent a further decrease in the weight of structures by eliminating the need for overlapping the materials in the joints. Additionally, if the use of flat tools is possible, it can be seen as a cheaper alternative to current processes.

1.3 - Objectives and deliverables

The main goal of the work presented in this document is to understand the applicability of the T-SPR technology to butt joining without auxiliary straps. Simplicity is a key driving motor of this research, by using tubular rivets of very simple geometry and a flat tool over which the riveting process is performed. This study approaches many aspects of riveting with this technique, having experimented with different rivet heights, thicknesses, sheet materials and a butt configuration with two coaxially fastened rivets. The objective is to provide a first contact with the presented riveting conditions of a butt joint configuration and a setup with flat tools (see Figure 1), setting foundations to carry out more detailed investigation and optimization in future work.

In Chapter 2, it is discussed the State-of-the-art, introducing the SPR technology. It is compared with other technologies commonly used in the automotive industry, relating some of their advantages and disadvantages. After that, some SPR variants are discussed, following the presentation of the T-SPR process and the rivet geometry used as the basis for this work. Chapter 3 refers to the Methods, where it is presented the work overview, the fabrication of the rivets and sheets used in the experiments, the setup of the riveting and destructive tests, and finally the processing of the data. Chapter 4 is the chapter of the Results, and there are presented all the results from the different tests along with some comments and considerations. The tests regard the response of the process to different rivets and sheet materials. Chapter 5 ends this document with the Conclusions, where the achievements of this work are compiled, and future work suggested.

Figure 1 – Section view of a butt joint between two aluminium sheets using T-SPR technology.

Chapter 2

State-of-the-art

As previously mentioned in the Introduction chapter, automakers face difficulties in joining dissimilar materials and non-ferrous alloys, ever more common in the structure of vehicles, with the well-established RSW. For this reason, joining by forming technologies such as SPR, clinching, or flow drill screwing (FDS) have gained their place on the shop floor. In section 2.1, self-piercing riveting will be presented regarding subjects such as the stages of the process, or methods for the quality assessment of the joints, along with a brief description of alternative technologies of clinching, flow drill screwing and RSW. In section 2.2, some of the technologies that are also present in the automotive industry are discussed, with a comparison between those and SPR. In section 2.3, it is given emphasis on some of the many variants and advancements in SPR technologies. In section 2.4, tubular self-piercing riveting and this study, in particular, are put in context with previous work. Finally, in section 2.5, the T-SPR rivet is presented along with the dimensions chosen as the basis for this study.

2.1 – Introduction to SPR

Riveting can be employed to join sheet metal by either cold forming, or hot forming processes, depending on the application. Often, is required to predrill the materials to join so that the rivet can be positioned and then plastically deformed to establish the connection. With later developments, some technologies allow the insertion of the rivet without a predrilled hole, so both the rivet and the joining materials suffer plastic deformation. This feature gave the respective technologies their name of self-piercing riveting. Since no chemical or phase changes occur during the process, riveting technologies are applicable to a broader range of materials, especially when compared to welding.

Self-piercing riveting has its origins in the decade of the 1960s, however it wasn't until the 1990s that the technology was widely researched and improved upon [2]. The automotive industry has been the main incentive to investigation of this cold forming process, with the first mass implementation of the process in the automotive production in 1993, with the Audi A8 [2]. From that point on, many other vehicle manufacturers extensively used this technology especially for the joining of aluminium alloys, used for weight reduction purposes and efficiency targets.

The conventional process of SPR consists of riveting together two, or more, sheets of material by pushing a rivet, usually at a fixed speed, into the overlapping materials without any pre-drilled or pre-punched holes. The deformation of the rivet's skirt (flaring), encouraged by its geometry and the shape of the die cavity, takes place inside the workpiece and is responsible for creating the mechanical lock that holds the sheets together. This is a cold-forming process, so it takes place at room temperature.

Li et al. [2] divide the SPR process into four stages: clamping; piercing; flaring; and releasing. First of all, the sheets are positioned, overlapping each other in the joining region, in what is called the joint stack. Then the riveting starts, and the machine clamps the sheets between the blank holder and the die (clamping stage), holding them tightly together in place for the consecutive stages. The applied clamping force may differ according to each particular joint stack. Higher forces worsen material flow of the bottom sheet and increase local work hardening, making the joint more prone to cracks around the joint button region [2], due to the higher friction levels. It follows the piercing stage, where the punch drives the rivet in its axial direction, perpendicular to the sheets' surface. The rivet is forced to pierce through the materials, until the bottom sheet is just partially pierced. During this stage the flaring is minimal. This step may be longer or shorter depending on the thickness of the joint stack and the hardness of the materials. As the rivet continuous being pushed, it faces resistance from the bottom sheet supported by the die, initiating the flaring stage [2]. While the rivet is set, it flares and makes the sheets further deform, filling the die cavity. For harder materials the flaring starts earlier than for softer ones. Not only the hardness of the sheets, but also rivet's hardness and geometry, as well as die geometry, influence significantly the flaring. This step creates the interlock required to hold the workpiece together. During the riveting, gaps between the sheets may occur, but as the punch keeps driving the rivet, it compresses the workpiece and any gaps will be reduced or even closed. Finally, when the threshold value of load or stroke is reached, it comes the release stage and the punch retracts from the joint, which gets an elastic recovery and the workpiece is released from the die. The whole process can happen quickly, with Böllhoff claiming cycle times under $1.5s$ with a fully automated system [3].

As mentioned, the joining of aluminium components was something that spread the SPR technology throughout the automotive manufacturers. However, the process has been used in a vast array of materials both in similar and dissimilar joints. Atlas Copco claims to provide their customers with self-piercing riveting systems that can join dissimilar joints such as aluminium to steel and composites to metals, as well as similar connections between aluminium alloys or steels [4]. But the scope extends to magnesium, copper, plastics, or wood, for example [2]. As Li et al. denoted, the joining materials need to fulfil at least two basic requirements to be joined by SPR. First, the materials require a minimum level of ductility, especially the bottom sheet, to cope with the high strains during the process. Otherwise, there will be cracks around the joint button, which significantly degrade the mechanical properties of the workpiece. Second, the hardness and strength of the materials need to be inferior relative to the rivet's, otherwise it will not pierce, or flare, as designed, compromising the interlock [2].

The quality of the riveted connections depends on many factors. Ang [5] managed to establish a cause-and-effect relation between some parameters of the connection and their effect on the joint's defects and failure modes, from the available literature. The list identified rivet material and geometry, sheets' material and thickness, friction between sheets, stacking sequence, die geometry, and loading conditions, as factors influencing the quality and behaviour of the joint.

Self-piercing riveting is often used in structural applications. Thus, it is very important to perform quality control in a regular basis, that is, to make sure that the riveting process is yielding reliable connections with the expected mechanical properties consistently throughout the whole production series. For this, there are destructive methods, which render the joined components unusable, and there are non-destructive testing methods (NDTs) that do not interfere with the functionality of the riveted joint. Common destructive methods are tensile-shear, cross tension and coach-peel tests, or even cross-section inspections. Cross-section inspections allow the measurement of key parameters that impact the joint's mechanical properties, for instance the riveted head height, h_h, the undercut, u, and the remaining bottom thickness, t_b, [6], illustrated in Figure 2.

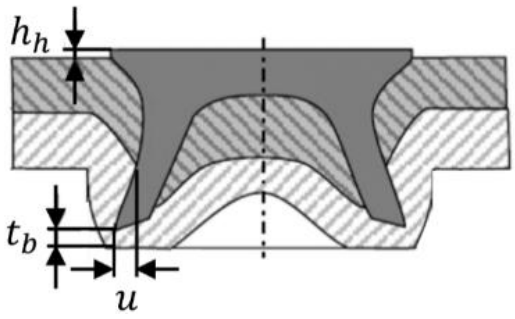

Figure 2 – Illustration of the cross-section of a SPR connection, depicted with the rivet's head height, h_h, undercut, u, and remaining bottom thickness, t_b. Adapted from [8].

Destructive tests are useful for the characterization of the mechanical properties of the joint under different loading scenarios and to predict failure modes and mechanisms. These tests can be used to assess if the process is performing as expected, based on the mechanical properties of randomly picked workpieces, but they often fall in favour of NDT methods for being more costly and time consuming than the latter [7]. Examples of NDTs are visual inspection, X-ray computed tomography, ultrasonic spectroscopy, or force-displacement curve analysis. Johnson et al. [9] used visual inspection for monitoring manufacturing errors. They used a computer vision system to automatically detect whether the riveting machine is loaded with none, one, or two rivets at once, before applying the setting force. Despite preventing cases where a rivet was not set, or two rivets were set on top of each other, this method does not detect quality defects of the riveted joint, such as lack of flaring or piercing through of the bottom sheet. To monitor the interior of the connection, Neuser et al. used X-ray computed tomography. The technology works by placing the workpiece between the X-ray tube and the detector and scanning it in different points of view, thus creating a volumetric image after computing all the projections with appropriate software [9]. This process allowed the authors to observe the full volume of the joint, thus providing a more complete diagnostic than cross-section inspection. However, this technique requires the analysis of an expert and is prone to human errors. A very common NDT method, used with automated systems by the automotive industry, is the force-displacement curve analysis. This method makes use of sensors to collect real-time data of force and displacement of the punch, to plot the connection's force-displacement curve

and compare it with a reference curve. The curve depends, among other aspects, on the joint stack and rivet used, so the reference curve changes for different joint parameters. If the process curve falls out from the reference curve, beyond a tolerance range, the joint is signalled as defective. This method is the quickest and most cost-effective solution. It provides quality assessment to every joint while the component is online, without adding cycle time to the riveting process. The downside is that the method states if a connection is admissible or not, without providing clear information about the parameters of the physical joint (i.e., interlock, undercut, etc). It is unlikely, but possible, that a joint with superior properties is labelled defective, because it falls outside the reference tolerance range. Therefore, the reference curve must be carefully selected, usually by cross-section analysis [2].

Ang identified four stages of a typical SPR force-displacement curve, represented in Figure 3. In the first, stage the punch load slowly increases, as the rivet forces downward and bends the sheets into the die. From the moment that the load induces more stress than the upper sheet's tensile strength, the rivet starts piercing the sheet [5]. As the section of the rivet's tip, piercing the sheet, increases, the punch load keeps increasing (section I in Figure 3). Stage II begins as the rivet starts penetrating the lower sheet [5]. In Ang's case, the load is kept approximately constant with a slight rising tendency during the piercing of both top and bottom sheets, since they are made of the same material. As the piercing takes place, the sheets' displaced material gradually flows into the die cavity [5] (section II in Figure 3). For a thicker upper sheet this stage takes more time. Stage III is marked by the rising of the load in a steeper slope. At this stage, the rivet's flaring is notorious and promotes the load increase (section III in Figure 3). A larger die cavity prolongates this stage. Stage IV is the final stage. The rivet head is set to its final position [5], as the force is further increased at a higher rate. The high load acting on the rivet drives any gaps between the sheets to close, increasing the amount of flaring and packing the materials into a tight joint with a mechanical interlock. This stage ends when the machine reaches the predefined load or displacement (section IV in Figure 3).

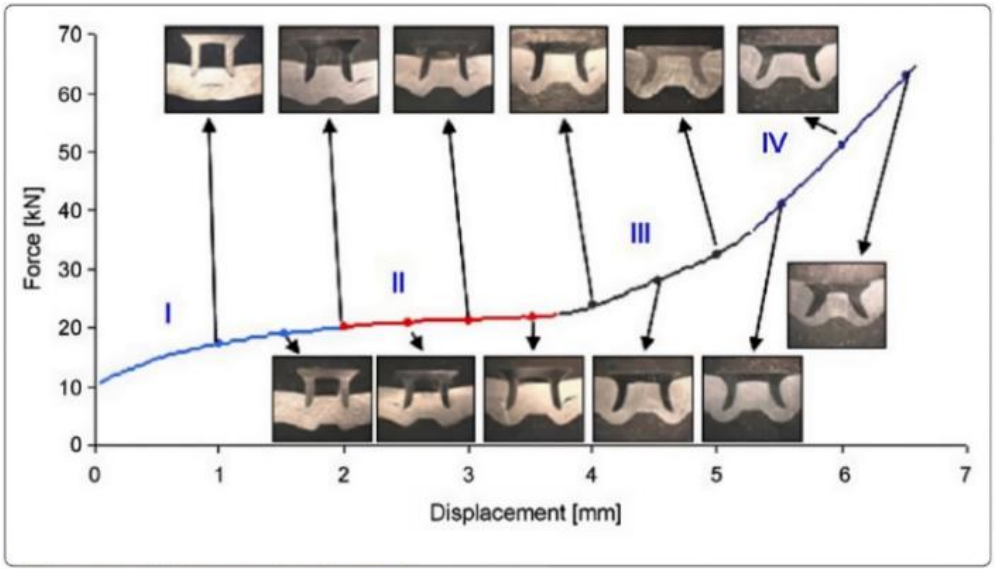

Figure 3 – A force–displacement curve of a SPR process [10].

There is a variety of machines available on the market to perform SPR connections. Manufacturers offer many solutions ranging from battery-powered hand-held tools, to stationary pedestals, or fully automated robots with die changing and condition assessment, rivet feeding and rivet positioning capabilities. The automotive industry tends to favour servo driven robotic systems over hydraulic driven systems due to the greater energy efficiency, good precision and repeatability [2]. Customers can choose the solution that better suits their needs depending on criteria like cost, level of automation, the required riveting force, joint accessibility, or projected production rate, among many others.

2.2 – Alternative technologies and brief comparison

Some of the concurrent technologies to SPR are flow drill screwing, clinching and resistance spot welding. These are briefly described below, followed by considerations about their advantages and disadvantages in relation to SPR.

Flow drill screwing consists of pushing down an element into the workpiece while spinning it, thus creating a joint. This operation locally generates heat and plasticizes the materials, hence the name “flow”, then pierces through the materials, “drill”, and creates its thread with which it fastens the sheets, “screwing”. It is a technology that only requires single-side access to the joining components. The fastener has a conical tip, a thread in the middle section, and a specially designed head that gives enough clearance to the material that flows upward during the fastening. This process can be divided into three stages (see Figure 4). In the first stage, the fastener is set spinning on top of the material, generating heat by friction. While spinning, the screw pierces through the workpieces making the materials flow up and downward along its tip. In this way, a channel is created whose length is greater than the thickness of the workpiece. During the second stage, a thread is formed in the pierced channel by plastic deformation. The final stage is the clamping of the head of the fastener to the upper component with the required torque for a secured connection [11]. The different stages of the process happen quickly allowing very high productivity, when automated, with Bölhoff [12] claiming cycle times in the range of 0.9 and 1.5 seconds between joints. Unlike clinching or SPR, these joints allow disassembly, due to the forming of a thread in the materials, which makes them easier to recycle [13].

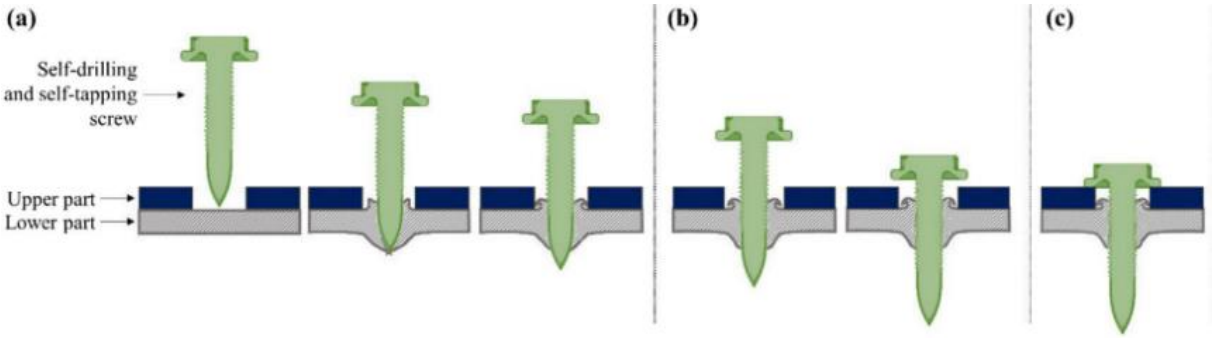

Figure 4 – Illustration of the process stages in flow drill screw driving: (a) heating, penetration, and bush forming; (b) thread forming and screw advancing; (c) tightening [11].

Clinching is a cold-forming process that does not make use of any fasteners to create a joint. These joints are therefore lightweight and cheap. This process requires a punch that presses the sheets into a die, shaped so that the material flow results in a mechanical interlock. Therefore, clinching requires access to both sides of the connection. The drawback is that the joints are weaker than those made by SPR for example. Kascak et al. tested both clinched and self-piercing riveted joints of the same materials with clinching joints achieving about 21-30% of the load that SPR joints sustained before failure [14]. Ren and Chen [15] introduced butt joining to clinching, making use of an auxiliary strap, in the die side, of the same aluminium AA5052 as the plates to join (Figure 5).

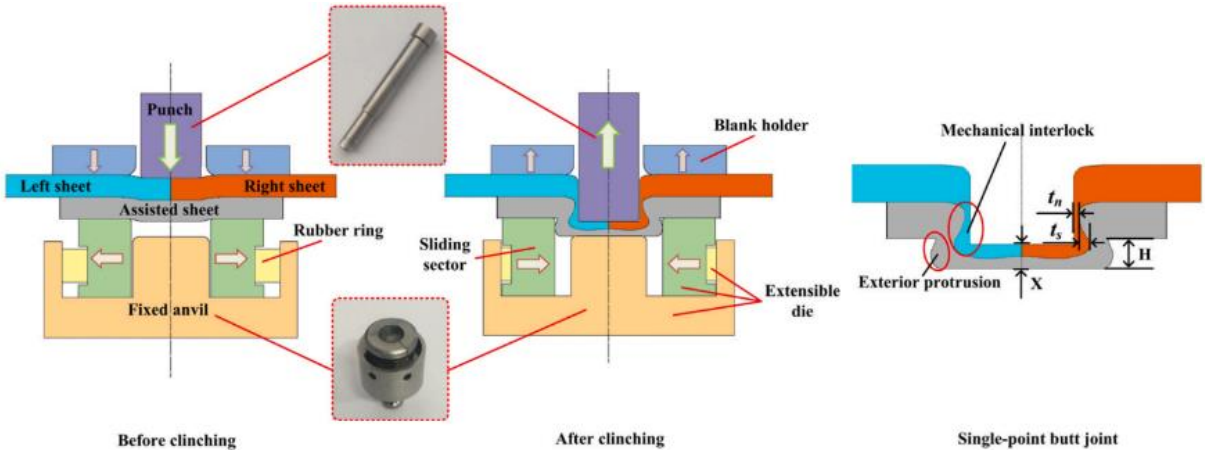

Figure 5 - Process of the single-point butt clinching [15].

As previously said, resistance spot welding is facing difficulties to meet the challenge of joining dissimilar materials and some aluminium and magnesium alloys. One key feature that characterizes this process is that the connection is secured by means of multiple small weld nuggets in different points, “spots”, of the assembly. The process works by clamping the sheets in between two electrodes and making a high current run through them. The current faces the most resistance in the interface of the sheets, thus generating an intense heat, according to Joule’s Law (Figure 6). The extreme heat then fuses the materials in a weld nugget between the overlapped materials. The joint is only finished after the weld nugget cools down and solidifies, while still maintaining pressure from the electrodes [16]. The cooling is provided by heat conduction from the workpiece to the two water-cooled electrodes, but also through dissipation in the workpiece [16].

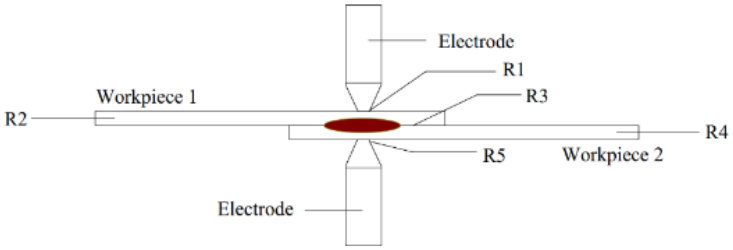

Figure 6 – Illustration of the electrical resistances in a sheet stack-up during RSW [17].

The clear advantage of SPR over RSW is the broader variety of materials that SPR can join, and the greater flexibility in joining dissimilar materials together in multilayer stacks. SPR dispenses the use of jigs to prevent the joined materials from distorting during thermal expansion cycles [21]. Moreover, the cold forming technology does not degrade the material properties due to heating [2], and dispenses any surface preparation operations, dealing well with coatings on the workpiece. Another important aspect is the absence of sparks, spatter and fumes during production with SPR, making it a cleaner technology. On the other hand, SPR requires higher setting forces than those used for clamping in RSW.

The major advantage of SPR over other riveting techniques, like solid or blind riveting, is the ability to join materials in a single step without any pre-manufactured holes, making it more tolerant to misalignments in the workpiece. SPR comes with the disadvantage of requiring access to both sides of the joint, unlike blind riveting or FDS, which may bring issues with inaccessibility or insufficient gun clearance. Clinching shares with RSW the advantage of not using fasteners, that increase cost and weight. In this study T-SPR is used to produce pure butt joints, that clinching and FDS cannot produce without an auxiliary overlapping strap. From the presented technologies, FDS is the only one that is not permanent, which can be positive from a recyclability standpoint but can also be of concern with unwanted unfastening.

SPR may be found in hybrid joints with adhesive bonding. The hybrid technology was found to increase the strength and energy absorption capabilities of the joint [18]. SPR brings the additional benefit of maintaining the bonded workpiece stable while the adhesive cures, lowering the production time.

Generalizing conclusions about the mechanical resistance of one technology in relation to another may be misleading and there are often contradictory conclusions. For instance, experimental results from Meschut et al. show that clinching withstands about 12% higher shear loads than SPR, when joining 2mm thick aluminium sheet to 1.5mm thick boron steel sheet [19]. Opposite to the above-mentioned results from Kascak et al. [14]. Han et al. [20] could not conclude definitively whether SPR or RSW provides the most resistant joints, after experimenting with both technologies in a back-to-back comparison. They concluded however, that the contradictory results found in the literature might be due to the fact that the results in SPR and RSW comparisons depend on the level of optimization of the process used on the tests and the loading geometry. Moreover, there are many variants of each joining technology better suited to specific cases. Consequently, joining technologies may provide better or worse mechanical properties relative to others depending on the given situation.

2.3 – SPR variants and solutions

SPR has branched into many variants developed for specific materials or applications. When it comes to further increasing the array of materials rivetable, one of the most prominent problems is that the materials are required to have a minimum amount of ductility, for being joined with a cold-forming process such as SPR. However, researchers have come up with many different variants of SPR that allow riveting low ductility and even fragile materials. In 2021 Wu et al. [18] compiled some of the latest developments in the field of SPR, referring the advantages and disadvantages of some of those processes. Generally, the solutions are based on either increasing the ductility of the materials via heat transfer mechanisms, or by changing the process mechanisms. Some of those variants will be briefly discussed below.

SPR joints with magnesium alloys are prone to show cracks in the lower sheet, because of the material's low ductility at room temperature. Durandet et al. [22] experimented riveting two overlapped sheets of magnesium alloy with a LASER-assisted self-piercing riveting (LSPR) system, supplied by Henrob (UK) Pty Ltd. Before riveting, a LASER hits the die facing surface of the joint's bottom sheet, pre-heating the material to over $200°C$. With this technique, the authors obtained connections without any visible cracks and good mechanical properties, unlike identical joints riveted without pre-heating. Even though the pre-heating step increases cost and cycle time, this process can be fully automated and allows a wider variety of materials to be self-piercing riveted.

He et al. [6] joined TA1 titanium alloy sheets, pre-heating them with an oxyacetylene flame gun up to $700°C$ to increase their formability. They riveted similar joints of titanium-titanium and dissimilar joints of titanium-aluminium (AA5052 alloy) and titanium-copper (H62 alloy), with the titanium both as top and bottom sheet. With this process the connections did not show any cracks. Additionally, the authors concluded that the stack order affects the mechanical properties of the dissimilar joints. For instance, in the titanium-aluminium joints, with the titanium as top sheet, the average peak tensile-shear load and energy absorbed until failure were $4.3kN$ and $10.2J$, respectively. While joints with the aluminium as the top sheet resisted an average of $3.8kN$ and absorbed $18.2J$ of energy.

Friction self-piercing riveting (F-SPR) comes as another approach to the problem of riveting low-ductility materials such as cast aluminium alloys, preventing cracking defects in the sheets. With this process, a rivet, similar to a conventional SPR rivet, is inserted into the sheets while rotating at a controlled speed. The friction between the rivet and the sheets creates heat which increases the ductility of the materials avoiding cracks related to high deformations [23]. F-SPR presents a solution based on heat transfer to the workpiece, like the processes above, however this variant has the advantage to produce connections with joining mechanisms of both self-piercing riveting and solid-state welding. The downside is a more complex machine and lower production rates. When riveting a sheet of aluminium over one of magnesium with conventional SPR, Li et al. [23] faced issues with cracking of the magnesium sheet. However, when setting the rivet by the F-SPR process, they successfully joined the materials without cracks, increasing the strength under tensile shear load

conditions from a peak load of 1.94kN with SPR to 3.98kN with the F-SPR variant. This process increases the parameters to adjust. Using this variant, the authors concluded that increasing the rotational speed decreases the interlock, however if the speed is set too low there are cracks in the materials.

Another solution to rivet fragile or low ductility materials is self-piercing-through riveting (SPTR). The main difference between this process and conventional SPR is that the rivet skirt flares and forms an interlock on the outside of the joint, below the bottom sheet. With this technique, the rivet pierces through the joining materials and reaches contact with the die underneath, where the skirt further flares, locking the materials between the rivet head and the flared skirt. In dissimilar joints, this process allows for the less ductile material to be either the top or bottom material. Rao et al. [25] joined two overlapping sheets of compression moulded discontinuous carbon fibre reinforced nylon 6 composite (30% mass fibre) with both STPR and conventional SPR technologies. They found that the STPR technique significantly improved the amount of interlock and the joints' mechanical properties relatively to the conventional SPR process.

There is plenty of investigation still being done on SPR. Liu et al. [26] investigated a new variant, called Padded self-piercing riveting (P-SPR), on joints between aluminium 6061-T6 and AM60B high-pressure die-cast magnesium, as bottom sheet. The proposed process consisted of applying SPR technology with the addition of a deformable and disposable steel pad between the die and the bottom sheet to relieve the latter from stress concentrations. When joining the materials with conventional SPR, the authors registered cracking in the joint button. However, the use of a steel pad in the new P-SPR process allowed the joining of these materials without defects.

The joint stack plays an important role on rivet and die selection. In addition to the ductility of the materials, the thickness of the stack also needs to be considered and might even dictate the feasibility of the joint. To circumvent this limitation, Alves et al. [21] suggested the use of a process they designated double-sided self-piercing riveting (DSSPR). The process makes use of a fully tubular rivet that is placed between the top and bottom sheets. While the punch drives the top sheet against the bottom, it presses the rivet inside. The rivet then pierces into the materials and flares inside the workpiece, thus creating the connection. With this process the rivet is hidden inside the workpiece, benefiting from protection against galvanic corrosion. From their experimental work with two-layer joint stacks, the authors concluded that this process can join sheets with large thickness, because it is independent from this parameter. Another advantage is that no dedicate dies or punches are required, as the tools only need to be flat, so the joints show no protrusions, unlike conventional SPR joints.

Regarding the recyclability of riveted components with SPR, efforts have been made to be able to use a rivet of the same material as the workpiece, for similar material joining. Hoang et al. [27] experimented joining, joint stacks of two aluminium sheets of $2mm$ thickness with different heat treatments, using aluminium rivets of different alloys. They concluded that, for some combinations of sheet and rivet alloys, it is possible to obtain a good connection and managed to achieve a maximum force 10% below that of using an identical rivet made of boron steel, under a combined loading of shear and pull-out solicitations.

2.4 – Tubular self-piercing riveting

This study comes in the sequence of previous work from Alves et al [21]. The authors started experimenting with a process which they called double-sided self-piercing riveting (DSSPR), using stainless steel rivets and aluminium sheets. It consists of joining two overlapped sheets with a tubular rivet, with chamfered ends, placed in between the materials. The advantages of this process were, for instance, the avoidance of protrusions, the protection of the rivet to galvanic corrosion, and the ability to join thick sheets, as the process was regarded as independent of the sheets' thickness [21]. Subsequent work concerns, for instance, the application of the process to the joining of different materials. Alves et al. [28] used the technology to rivet polymer sheets. Initially, they faced difficulties, because the rivet would pierce the sheets with insignificant flaring. Because of that, they introduced a new geometrical parameter to the rivet, which consisted of making the edge of the chamfers blunt with a radius of $0.2mm$, thus increasing in large measure the interlock and mechanical properties of the joint. Further experimentation with materials included the use of DSSPR in dissimilar polymer-metal joints by Pereira [29]. The author tested different variations of the DSSPR process that would allow the joining of a PVC sheet to one of an aluminium alloy, using a stainless steel rivet. The variations went from differentiating the chamfer angle of each end of the rivet, to a two-stroke process piercing each material at a time, or even pre-machining a flat cavity in the aluminium for increased symmetry of the interlock and piercing depth of both materials. This present study follows the series of developments in DSSPR technology, looking into new applications for the tubular rivet design. The goal is to evaluate to what extent is possible to join two sheets in a butt configuration instead of an overlapped one, making use of tubular rivets that are identical to DSSPR rivets, except for the fact they present one chamfered end instead of two. Some of the lessons learned by previous authors using DSSPR are applied to this study such as the blunt chamfer edge geometry, the most adequate chamfer angle, and the dimensions of the first rivet used in this study, which come from the applicability window respective to DSSPR, presented later in this document.

This study presents the tubular self-piercing riveting (T-SPR) process, which is much like conventional SPR in the sense that the rivet pierces the materials from one side of the workpiece, in a single stroke, however it uses the tubular rivet geometry, hence the name tubular-SPR. The main distinction between SPR and T-SPR rivets is that the latter are completely hollow inside, as a tube with a chamfer, whilst the former are blind and often called semi-tubular.

T-SPR shares the advantages and disadvantages of conventional SPR. It can be used in automated systems, benefitting from automated quality control, alike general SPR technologies, via the comparison of the force-displacement curves with a reference. As a SPR variant, it does not require pre-drilled holes for the fastening of the materials, but is bound to joining sufficiently ductile materials ate room temperature. Moreover T-SPR does not lead to waste material during the riveting process, unlike blind riveting, however it is necessary to have access to both sides of the workpiece.

2.5 – Rivet geometry

In 2001, Kato [30] presented a new type of rivet, called pipe rivet, the geometric parameters of which he identified. They are the rivet's height, h, the external diameter, d, the thickness, t, and the chamfer angle, α, (relating to the rivet in its undeformed state). These parameters are also applicable to the T-SPR rivet used in this study, illustrated below in Figure 7, and they impact the quality and mechanical resistance of the joint. Additionally, when the rivet presents a very large difference in mechanical strength relative to the materials in the workpiece there might be problems with the lack of a mechanical interlock. In such cases, it is important that the chamfer tip, in the rivet's skirt, is deburred to a certain width, c, which will be named tip width. Alves et al. [28] found this parameter important for the flaring of the rivet when joining $6mm$ thick PVC polymer sheets with the process of DSSPR. With a sharp chamfer edge, the connection failed, as the rivet did not produce a mechanical interlock. That is because the rivet is made of AISI 304 stainless steel with a much larger mechanical strength relative to the polymer of the sheets, piercing through with negligible flaring. They solved this problem and achieved a satisfactory interlock by blunting the chamfer edge, with a $0.2mm$ radius. Based on those results, the rivets used in this study have a flat rivet tip of $c = 0.2mm$. The tip is flat, due to practical difficulties of making a radius with precision.

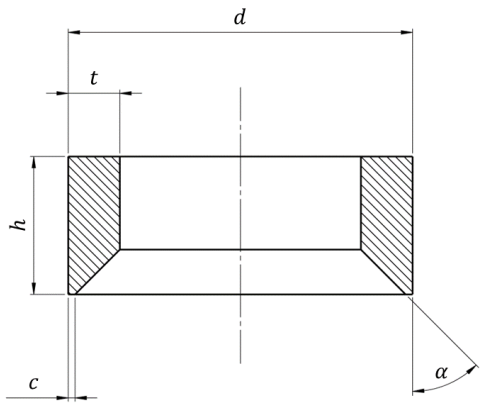

Figure 7 – Section view of the T-SPR rivet and its dimensional parameters.

The chamfer angle has an impact on the flaring and thus the interlocking of the rivet. Alves et al. concluded that for the tubular rivet of DSSPR the chamfer angles that provide the best interlocking to the connection of aluminium sheets are $30°$ and $45°$ [21], although the $45°$ angle comes with the cost of higher energy spending for the riveting process. In 2017, destructive experiments of overlapped 6063 aluminium sheets riveted with a flange-type tubular stainless steel rivets (Figure 8a) led Huang et al. [31] to the conclusion that the chamfer angle of $45°$ (represented by θ in Figure 8b) allowed the joints to resist the highest loads under tensile-shear conditions. The comparison was

between rivets with chamfer angles of $30°$, $45°$, $60°$ and $90°$. For these reasons, all the rivets used in the present work were machined with a $45°$ chamfer angle.

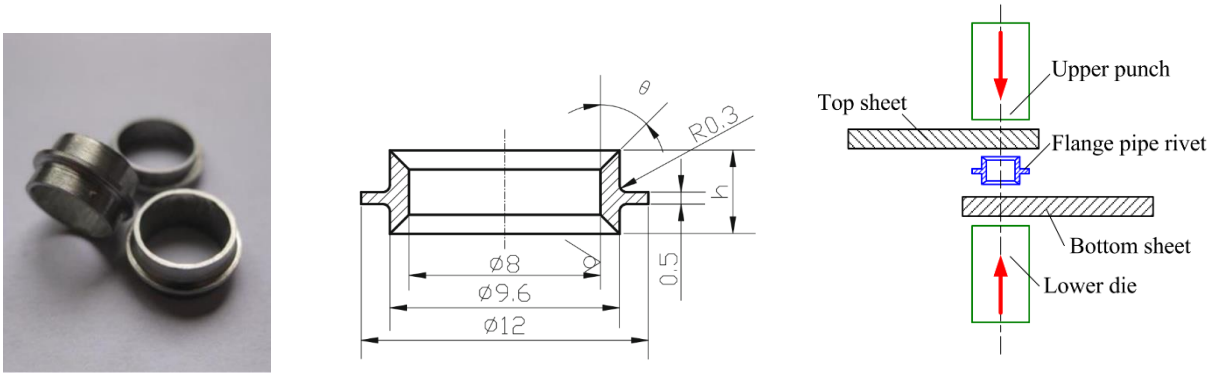

(a) Flange-type rivets. (b) Rivet's dimensional parameters. (c) Riveting process illustration.

Figure 8 – Flange-type tubular rivets.

Rita [32] managed to establish the applicability window of the DSSPR process that results in a successful joint between two aluminium workpieces of equal thickness of the AA5754-H111 aluminium alloy (the same as the present work), joined by a stainless steel (AISI 304) rivet with $10mm$ external diameter and $45°$ chamfer. With his experimental work and data gathered from previous studies under the same conditions, he found a relation between rivet height, rivet thickness and workpiece thickness that serves as a starting point for the selection of a rivet that provides a quality connection (Figure 9).

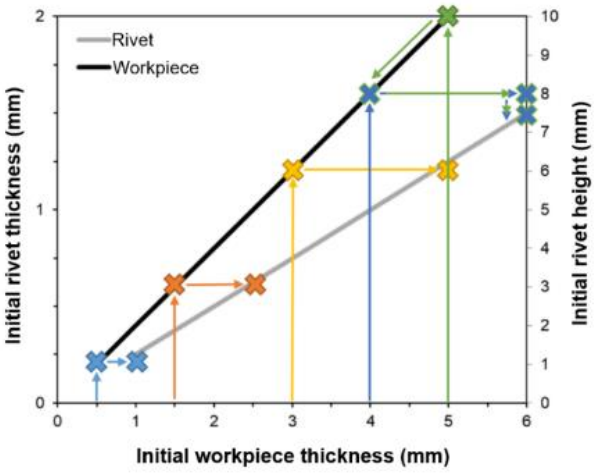

Figure 9 – DSSPR process window for rivets with 10mm external diameter and 45º chamfer angle, in joints of similar thickness sheets [32].

During the DSSPR process, the rivet pierces both upper and lower sheets simultaneously. When completely set, one-half of the rivet's height is inside the upper sheet, and the other half is inside the lower sheet. Both the top-half and the bottom-half of the DSSPR rivet are, in theory, identical to a full T-SPR rivet with half the formers' height. Hence, the DSSPR process can be described as two T-SPR processes occurring simultaneously with a symmetry plane perpendicular to the DSSPR rivet's axis and crossing it at half its height. Figure 10 illustrates this assumption.

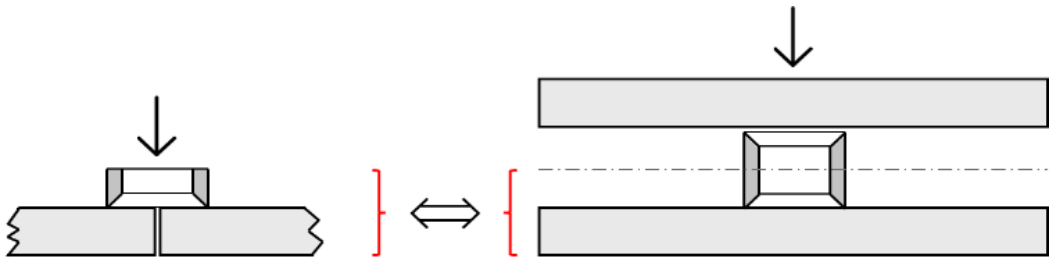

Figure 10 - Assumption of equivalence between T-SPR in a butt joint, at the left, and conventional DSSPR, at the right.

Considering what has been noticed, a good starting point for the experimental procedure of T-SPR joining is to select a rivet with half the height of the one deduced from the applicability window (valid for DSSPR rivets). The deduction based on Rita's applicability window, in Figure 9, begins with the statement of the workpiece's thickness (on the abscissa axis), which is $5mm$, in this case. Therefore, one follows the green vertical arrow, in Figure 9, that starts on the $5mm$ abscissa, until reaching the respective point in the black line, signalled by the green cross. That point indicates that the suggested rivet thickness would be $2mm$ and the height $10mm$ (read on the left and right ordinate axis respectively). Despite that, the author notes that, for workpieces thicker than $4mm$, the rivet of $1{,}5mm$ thickness and $8mm$ height, leads to good results, based on experimental tests. Hence, in Figure 9, from the green cross the figure presents another arrow pointing to the blue cross below respective to $4mm$ thick workpieces. Having said that, the DSSPR rivet selected for joining sheets with

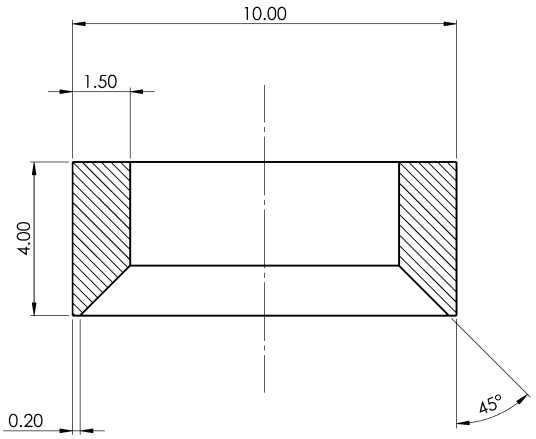

Figure 11 - Dimensions on the section view of this study's standard rivet.

$5mm$ thickness, would be one with a thickness of $1.5mm$ and a height of $8mm$. Consequently, a suitable T-SPR rivet for joining the same sheets would have the same $1.5mm$ of thickness and a height of $4mm$, so that was taken as the standard rivet with which this study was based upon. The window was developed from results using AISI 304 rivets, while the present work makes use of AISI 316L alloy rivets. Nonetheless the difference in properties between the alloys is small, with the 316L showing slightly more ductility, so it is disregarded at this stage. The rivet taken as the standard, on which this study unfolds, is shown with its dimensions in Figure 11, where the linear dimensions are displayed in millimetres and the angle is measure in degrees.

The industry offers a range of rivet materials including brass, aluminium alloys, stainless and high-strength steels. In any case, rivets made of steel alloys are the most common [2]. Often, rivets are subjected to heat treatments to improve their hardness, tailored for each particular application. In addition, rivets may also come with a coating, to improve corrosion resistance, to reduce friction with the workpiece during riveting, or simply for aesthetic reasons. There is a wide selection of coatings available such as zinc plating, aluminizing, or electroplated zinc-nickel, to name a few [33]. In this case the rivets have no surface treatment or coating.

Tubular rivets are already available in the market by companies such as Henrob, which provides a variety of rivet shapes and sizes including a tubular rivet, T-Rivet, with a design that differs from the rivets used, by having a countersunk head. According to Henrob, those rivets provide joining with reduced material displacement, allowing the joining of low ductility aluminium without button cracks in thick multi-layered stacks [34].

Chapter 3

Methods

The new application of the T-SPR process on butt joints motivates a wide range of tests to carry out to assess the mechanical resistance provided by this type of connection. This chapter starts by presenting an overview of the work developed and then proceeds to cover all the topics regarding rivets' and sheets' fabrication, and the development of the riveting and flexural testing setups, finishing with the explanation of the results' data processing.

3.1 – Work overview

This study's testing campaign started by riveting two aluminium sheets, using a rivet whose geometrical parameters are based on previous work, as described in section 2.4. The resulting connection revealed that the sheets separated from each other during the rivet setting. Therefore, the first task was to develop a setup that would ensure the correct joining of the sheets, as will be described in section 3.4. Later, the setup was modified to also enable the carrying out of flexural tests. The development of the riveting setup allowed the joining of two aluminium sheets in a butt joint configuration with the T-SPR process. The results of that development will be presented in section 4.1, as well as the analysis of the riveting curves obtained.

Changes to the rivet geometry were planned for subsequent tests. The first object of testing was the rivet thickness, t, (see Figure 7). Section 4.2 regards the joining and destructive testing of joints with rivets of various wall thicknesses. The objective was to understand in what way the rivet's thickness influences the quality and mechanical resistance of the workpieces, by using a rivet with a different thickness in each test. For this, the material and dimensions of the sheets and all the remaining geometric parameters of the rivet, such as the height and chamfer angle, were kept the same throughout the testing series. In this work, the quality is assessed by evaluating a set of features present in the joint after riveting, namely, the rivet interlock, the existence, or not, of protrusions or cracks in the joined materials, and the interface gap between the sheets. The second object of study was the rivet height, with the objective of understanding to what extent the height of the rivet, h, (see Figure 7) impacts the quality and resistance of the connection, once again, keeping all the remaining parameters unchanged. The results from the height tests are discussed in section 4.3. Even though the planned focus of this study was on the thickness and height of the rivets better suited for the riveting process, there was additional investigation unfolding on other aspects according to the results during the experimental campaign. Those aspects are related to the rivetability of different sheet materials (section 4.4) and a joining method for improved mechanical properties under tensile-shear loading (section 4.5).

The connections produced were analysed in terms of joining feasibility, through physical riveting tests, and mechanical resistance, via destructive tests. The destructive tests consisted mostly of tensile-shear tests, with some joint types also being subjected to flexural tests. Additionally, some workpieces were section cut to have the interlock and the gap in the joint's interface measured with a toolmaker's microscope. The setup and machines used are presented with more detail in section 3.4. Figure 12 summarizes graphically the work and experimentation done in the scope of this dissertation.

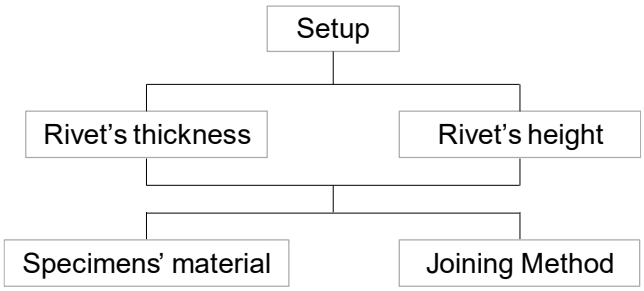

Figure 12 - Study overview.

3.2 – Rivets' fabrication

The rivets were extracted from a tube of stainless steel AISI 316L with $10mm$ outside diameter and wall thickness of $1.5mm$. Each rivet is obtained through a sequence of steps that involves machining operations in a lathe and sanding. The lathe used is manual with a three-jaw chuck, located in the Laboratório de Tecnologia Mecânica (LTM) laboratory. Before starting machining, a section of the stainless steel tube is cut with a metal bandsaw and inserted in the chuck of the lathe. Then, the first operation in the lathe is to chamfer the end of the tube with a chamfer angle of $45°$, which was deduced from the literature review. Next, the chamfered edge is deburred, so that later the rivet fits in the dedicated holder. After that, it follows a cutoff operation that determines the rivet height. The cutoff comes after the chamfer operation to achieve better height tolerance (Figure 13a). The tube is then removed from the chuck and replaced by the rivet, just cut off, and the holder that secures it. The holder is necessary so that the rivet is secure, whilst it does not get damaged or deformed with the clamping force of the jaws in the subsequent steps (Figure 13b). The rivet is then positioned in the holder with the chamfer facing the chuck and the chip from the cutoff operation is removed with a turning tool. Next, it is carried out the boring operation that determines the rivet's wall thickness using the corresponding drill bit size. Rivets with the same wall thickness as the original tube ($1.5mm$) are still re-bored with the matching drill bit to remove any remaining chips from the previous operations. Finally, the rivet is ready after lightly sanding off the chamfered edge (Figure 13c). As previously mentioned, this step removes very little material to ensure the correct deformation and flaring of the rivet even when riveting much weaker materials. The manual machining of the rivets, led to dimensional differences, namely in rivet height, which were visible during the results analysis of the riveted joints. The mass production of this type of rivet, for instance by multi-blow cold forming

commonly used for SPR rivets [2], would bring serious advantages relatively to the manual process, regarding cost and time, while improving the dimensional accuracy of the mechanical fasteners.

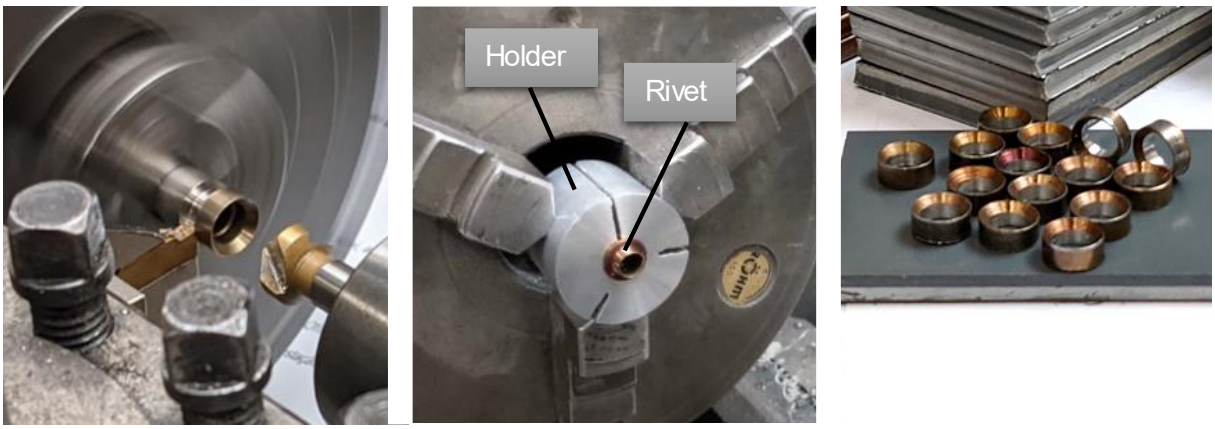

(a) Cut-off operation. (b) Rivet in Holder. (c) Finished rivets.

Figure 13 - Manufacturing of the rivets.

3.3 – Joining materials and sheets' fabrication

This study was conducted using mostly aluminium sheets as the joining material. Nevertheless, other materials were also riveted to understand the suitability of the process to different joining materials. The number of tests is limited, due to time constraints, so the sheets are made of two types of metals and one polymer. One of the metals is an aluminium AA5754-H111 alloy, over which this study was centred. The material was chosen for its wide use from the automotive to the shipbuilding and food industries, and for being characterized by very good formability and corrosion resistance [35]. The other metal chosen was commercially pure copper. This material has greater mechanical resistance than the aluminium used. Among other aspects, it is very important for the electrification of a growing number of products and machines, as in wirings, motors and busbars, with applications extending from heat exchangers to buildings' roofing and façades, for example. Finally, a polymer was selected to extend the scope of materials beyond metals. PVC is a widely available material common in various industries for its chemical resistance, electric insulation and easy fabrication properties. It can be used as either rigid or flexible grades, in many shapes and densities. In this case, it is a $1460\,kg/m^3$ rigid sheet PVC. This polymer has much lower rigidity and strength than aluminium, and so it provides a good extreme case to evaluate how broad the range of joinable materials is with this process while using stainless steel rivets. The materials were used in the same conditions as they were supplied, without any additional heat, mechanical, chemical, or surface treatments. All the selected materials have good formability at ambient temperature, so there were favourable conditions to test the process without any heating stages or other intermediate steps that would introduce complexity to the riveting process. The mechanical properties of the materials were obtained from different sources, [36], [37] and [38] for the aluminium, copper, and PVC respectively, and these are displayed in Table 1.

Table 1 - Mechanical properties of the sheets' materials

Material	AA5754-H111	Copper	PVC
Elastic modulus, E [GPa]	70	115	3.0
Yield strength, σ_y $[MPa]$	80	69-365	-
Ultimate strength, σ_u $[MPa]$	190-240	221-455	41.4
Density, ρ $[\mathrm{kg/m^3}]$	2700	8960	1460
Hardness Brinell [HBW]	52	86-100	15

The joining materials are sheets with $5mm$ thickness, $75mm$ long and $50mm$ wide. All the sheets have the same dimensions, so the effect of changing the sheets' dimensional parameters was not an aspect analysed in this study. The length of the sheets is such that it provides a safe distance between the joint and the clamping region for the tensile-shear tests. The width allows enough clearance between the rivet and the sheets' lateral edges, not to affect the riveting deformation mechanisms or cause joint failure due to stress concentration effects. All the aluminium, copper and PVC sheets were cut to size from the supplied materials without any additional treatments or finishing operations. The machine used was a RICO® HGR vertical cut guillotine shearing machine from the LTM laboratory in the university's facilities. Because of the guillotine's blade gap, this cutting process rounded the sheets near the cut edges, making the lateral faces of the sheets no longer planar and perpendicular to the sheets' base. Since the sheets interface each other with these surfaces in the riveting of the butt joints, the non-perpendicularity makes these faying surfaces not parallel to each other, thus reducing the joint contact area. Even though this might have some influence in the joining mechanisms, and consequently in the joint's mechanical properties, in practice there was no noticeable evidence of that influence justifying other method for cutting the sheets.

3.4 – Setups

The characterization of the joints on their feasibility and the comparison of the joints mechanical properties are based on the results coming from three types of tests implemented. They were riveting, tensile-shear, and three-point bending flexural tests. The riveting tests provide information about the force and energy required for joining two sheets, and about the resulting quality parameters for each connection. The tensile-shear tests aim to know the mechanical resistance of the connections when subjected to a load pulling apart the sheets in the longitudinal direction of the joint. Finally, the flexural tests were performed to a small number of joints as an assessment of the impact the direction of the bending moment caused by the applied force has on this type of joints. Both tensile-shear and flexural tests provide information about the force and energy applied, as well as the failure mechanisms of selected connections. The three types of tests were performed using a setup adapted to each one. The different setups are described with detail in the following subsections.

3.4.1 – Riveting setup

The setup used for the riveting tests was subjected to three iterations, taking corrective measures after each one. This was done by riveting aluminium sheets with stainless steel rivets, until it was possible to reliably obtain good quality joints. The initial setup was constituted by the machine, compression plattens, two sheets and a rivet. The compression plattens are screwed to the machine, one to the table and the other to the movable crosshead. The sheets are placed over the bottom compression platten without any fixture and the rivet is placed by hand on top, centred with its axis coincident with the sheets' interface plane and the chamfer facing the sheets. The setup was put to test by riveting two aluminium sheets with a rivet of dimensions derived from the applicability window, as described in section 2.4. The results of this connection were unsatisfactory and motivated more testing to develop a suitable setup for the process. The problem was a large gap created in the interface of the sheets during riveting. Because of that, the sheets required a device to restrain their separation movement in the longitudinal direction, perpendicular to their interface. The SPR machines available in the market come with a blank holder, often through which the rivet is fed. That could give some restraint by friction to the sheets' separation in the area surrounding the rivet. Unfortunately, the machine used was a universal testing machine without any kind of sheet holding device, and the installation of such would be too complex and expensive.

An alternative to having a blank holder is to include a support for the sheets, that prevents the separation phenomenon from occurring. For this, it was selected a block of steel, much more rigid than the sheets. A pocket was then machined in the centre of the block to sit the sheets, deeper than the sheets' thickness and $150mm$ long (the length of the two sheets in front of each other, i.e. butt configuration). The block had no lateral margins, because it was the same width of the sheets, $50mm$. In this way, the sheets are restrained inside the pocket only with the longitudinal direction blocked by the margins of the support left by the pocket operation. This solution turned out not to be viable, because the sheets have small variations in length, from the cutting process. On the one hand when the sheets are shorter than the pocket, it creates a gap. On the other hand when the sheets are longer, they do not fit. Therefore, the support needed to adapt to the dimensional variability of the sheets. The solution found consists in increasing the length of the pocket and bore two threaded M8 holes in one end of the support to fasten two screws. The screws would tighten the sheets against each other and against the other margin of the support on the longitudinal direction, regardless of the dimensional accuracy of the sheets. The setup was put to test, by riveting two aluminium sheets, with the support over the bottom platten and the sheets in the pocket cavity tightened by the screws. The resulting connection still exhibited a significant gap. This time, the separation force was such that the two screws indented the sheet they contact with, with an indentation depth approximately the same as the gap created in the interface, not preventing the interface gap. A final iteration of the support, represented in Figure 14, consisted of eliminating any chance of indentation by inserting a steel stop plate between the screws and the sheet they contact with, thus distributing the load over the entire width of the sheet. Another riveting test was carried out, and this time the results were positive with a very small interface gap. The support withstood the loads of the process without any damage or any

measurable plastic deformation. In conclusion, the support was stiff enough to withstand the riveting forces and to ensure good process repeatability, so the setup was fully defined for the remainder of this work. It consists of the machine (an Instron SATEC™ 1200KN, located in the LTM laboratory, the plattens and the support, as shown in Figure 14. With this setup, there is not a clamping stage where the sheets are vertically compressed before riveting starts, as found in commercial SPR systems with blank holding devices. Before riveting, the punch is lowered until it lightly touches the rivet already positioned on top of the sheets, as in Figure 14.

The riveting tests were conducted with a punch speed of $10mm/min$. For safety, both load and displacement limits were used as end test criteria. The displacement limit corresponds to the rivet height plus $1mm$, to ensure the rivet is completely set into the workpiece while accommodating any slacks in the system. The load limit used depended on the joining materials and the rivet's geometry. As found in previous work by Pereira [29], with DSSPR, materials with higher mechanical resistance require higher riveting loads due to the extra resistance to piercing and flaring of the rivet, so the end test criteria had to be adjusted accordingly.

Figure 14 - Riveting setup: at the left is the machine and plattens; at the right is a close-up view of the steel support with two aluminium sheets and the rivet positioned.

3.4.2 – Tensile-shear setup

Tensile-shear tests were used not only to determine the maximum load the workpiece withstands when facing a force solicitation under those conditions, but also the energy absorbed by the connection and its failure mechanism. These tests are analogous to the lap-shear tests often used to characterize SPR joints, with the difference that the joints are in a butt configuration instead of being

overlap connections. The tensile-shear tests were performed with an Instron 5900R universal testing machine, with mechanical wedge action tensile grips, located in the Laboratório de Caracterização Mecânica de Materiais laboratory. Relative to the Instron SATEC™ 1200KN, used for the riveting tests, this machine provides better precision data, with less noise, in the expected range of loads the workpieces might resist. The crosshead speed was set to $5mm/min$, and the end test criteria is a "Sensitivity" value of 50%. The test ends when the load drops by the "Sensitivity" value (within a time period of $100ms$), or when it is verified the complete separation of the rivet from one of the sheets.

3.4.3 – Three-point bending setup

The riveted connections are asymmetric in the sense that the underside is different than the upside of the workpiece, through which the rivet is inserted. This asymmetry might reveal different load bearing capabilities of the connection when subjected to bending moment depending on its direction of application. With an interest on understanding the response of the joints under these loading conditions, three-point bending flexural tests were conducted. The machine used for those was the same used for the riveting, but the setup had to be adapted. For that, it was used the same support as for the riveting, but with modifications. Two grooves were machined on the bottom surface of the support with $100mm$ between each other. The support was flipped with the upside down, positioned with the pocket cavity in contact with the bottom platten. Then, two stainless steel cylinders with $30mm$ diameter were put over the grooves. The workpiece sits on top of the two cylinders and is positioned by aligning it with dedicated markings. Finally, a third cylinder, identical to the aforementioned, is placed on top of the joint and centred over the sheets' interface. Figure 15 shows the setup used for the flexural tests. This solution allowed the use of the same support both for riveting and flexural testing without compromising the results of either.

Figure 15 - Close-up view of the flexural tests' setup.

3.5 – Data processing

3.5.1 – Compensation of the force-displacement curves

The Instron machine used for riveting and flexural testing provides data of force applied and punch displacement at time intervals based on user defined data acquisition settings, in this case every $200ms$. With these values, one can plot the riveting curve (i.e. the force as function of the punch displacement) and analyse it. However, those values do not correspond exactly to what the rivet undergoes during the process, because they are affected by the setup and the machine used for the process. In order to get the true displacement of the rivet, one needs to know the characteristic curve of the machine. For that, the machine was assembled with the setup of the process and set running (without the sheets), until it reached a threshold value of load, greater than the values used for the riveting experiments. The resulting curve was then downloaded from the machine's software to be processed. Using a calculation spreadsheet, it was possible to approximate the array of data points with a polynomial function. This function fits the data points in the range of the riveting loads of this study, that is known from the riveting experiments. The characteristic curve accounts for the rigidity of the whole setup, including the machine, as well as slacks and friction in the system. To get the rivet's true displacement for any given load, one must subtract the characteristic curve to the downloaded curve of the riveting process. The approximation polynomial function has a maximum absolute error of $0.011mm$ relative to the original data points, with a range of applicability from $0kN$ to $165kN$, thus covering the load values of all the different riveting curves. All the comparisons and results of setting force and energy mentioned in the next chapter relate to the true displacement curves, named in this document simply as riveting curves.

For the case of tensile testing the same procedure was adopted. However, in this case it was required the use of a sheet, ideally with infinite elastic modulus. Instead, it was used an aluminium sheet to get the characteristic curve of the machine. Despite being far from ideal, that did not alter significantly the results and the quality of the conclusions, which are comparisons between the different tests. The range of the approximation polynomial function for the tensile-shear tests is between $0kN$ and $3kN$, with a maximum absolute error of $0.002mm$ relative to the compensation curve's data points.

The characteristic curve of the flexural setup was approximated by a polynomial function ranging from $0kN$ to $1.8kN$, with a maximum error of $0.010mm$. The force-displacement curves from the three-point bending flexural tests required additional treatment. The results suffered from noise, since there is a big difference between the load values that the connections resisted and the load capacity of the load cell. To minimize the noise, it was used the "Exponential Smoothing" function from Microsoft Excel, with a "Damping factor" of 0.7. The values of maximum supported load and absorbed energy were calculated based on to the smoothed curves.

3.5.2 – Extraction and calculation of the results

For comparison reasons, and because the actual height of the rivets does not correspond exactly to the nominal height, it was assumed that the riveting force corresponds to that measured in the transition between stage III and stage IV of the riveting curve for each case, i.e. the point where the overload of the workpiece begins. That force is named the setting force and it will be used to compare the different riveting cases. Figure 16 illustrates the marking of the setting force ($72.62kN$), signalled in the riveting curve.

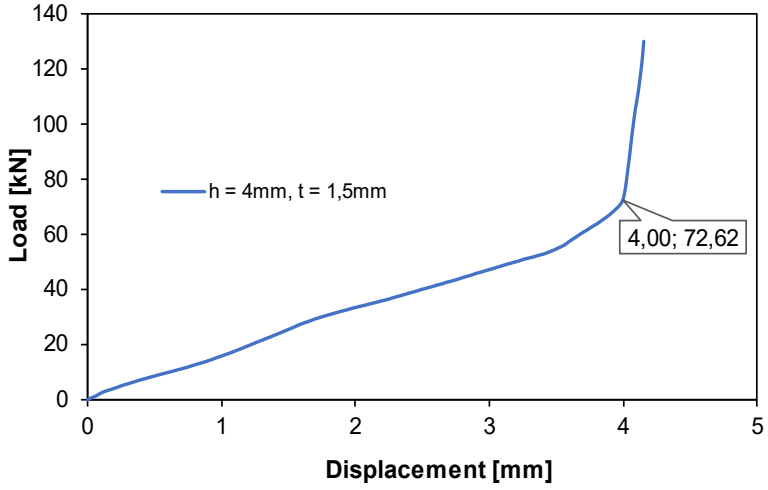

Figure 16 - Riveting curve with rivet's setting point.

The riveting energy calculation only takes into account the work done by the force that the punch applies to the fastening of the rivet, so it is based on the compensated curve. Considering the rivet as a particle, the general expression for work may be presented as follows in Equation (1), where W_c is the work transferred to the rivet, by the action of a force vector, $\vec{F}$, along a trajectory, C, and $\vec{r}$ is the displacement vector.

$$W_C = \int_C \vec{F} \cdot d\vec{r} \tag{1}$$

In this case, the trajectory is linear and the force acts in the same direction as the trajectory, so vectors $\vec{F}$ and $\vec{r}$ can be replaced by the product of their scalar values F and r respectively. It also means that the energy transmitted to the rivet corresponds to the area under the riveting curve. To better compare the results of the different connections, the energy consumption was calculated along the trajectory from $0mm$ to the displacement value corresponding to the setting force, d_S, of the respective connection. That being said, the Equation (1) can be written as follows in Equation (2):

$$W_c = \int_0^{d_S} F(r)dr \tag{2}$$

Finally, because the data acquisition is not continuous but rather an array of discrete values, the integral is in practice approximated by a summation, as shown below in Equation (3), where n is the number of data points.

$$W_c = \int_0^{d_S} F(r)dr \approx \sum_{i=0}^{n-1} \frac{F_i + F_{i+1}}{2} \times (r_{i+1} - r_i) \tag{3}$$

The summation consists of the product of the average force magnitude between two consecutive points and the distance the rivet moved on that interval, for each index, i, until the second to last data point. This procedure for the energy calculation was implemented also for the curves resulting from the destructive tests.

After riveting the sheets, the interlock was measured with a toolmaker's microscope equipped with digital micrometer screws. For that, the riveted connections were milled until cutting the rivet in half, to expose the diametral section of the joint. The sectioned workpieces were then taken under the microscope. The interlock, i, was not directly measured, but rather calculated as half the difference between the measured diameter of the flared skirt, D_s, and the diameter of the rivet's head D_h, shown in Equation (4):

$$i = \frac{D_s - D_h}{2} \tag{4}$$

This procedure averages any asymmetry of the interlock between both sides of the section. It is worth noticing that, even though the section cutting and the microscope measurements were carefully done, these are prone to human error. Figure 17 illustrates a cross-section with the nomenclature adopted in Equation (4).

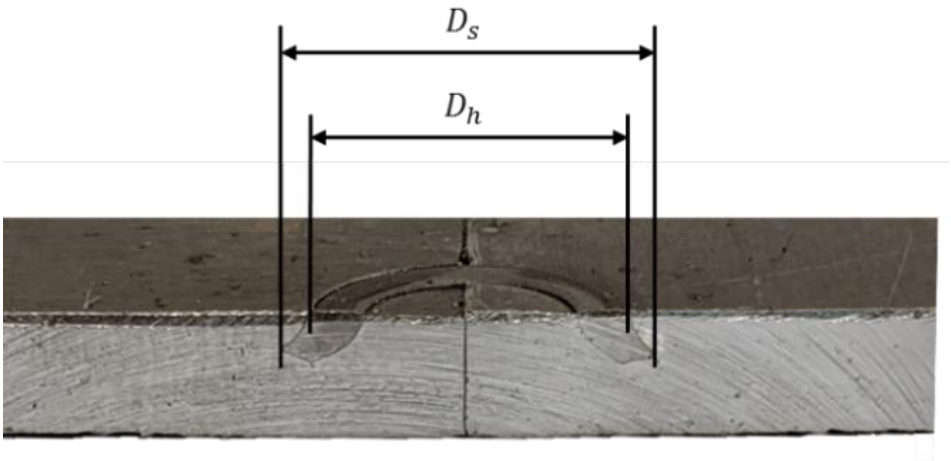

Figure 17 – Measured features for interlock calculation.

The joints revealed a gap in the interface of the sheets. This gap was measured with the same toolmaker's microscope used for the interlock assessment. For each joint, the gap is measured in two places, G' and G'', at half distance between the lateral edge of the workpiece and the rivet's perimeter. Figure 18 illustrates the two measurement points in the workpiece riveted without support for better visualization, as the remaining connections have gaps too small to exemplify. The value taken for the interface gap, g, is the average of the two measured values, G' and G'', as shown in Equation (5):

$$g = \frac{G' + G''}{2} \tag{5}$$

Figure 18 – Illustration of the points used for the gap measurement.

Chapter 4

Experimental results

Some of the most important factors characterizing cold forming processes are the load required to join the materials (in this case, the riveting force), the energy consumed to produce the joint, and the translation of those parameters into the strength and energy absorption capabilities of the connections. The focus of this study is the joinability assessment of butt joints with the T-SPR technology. Therefore, force and energy spent during riveting were established as the highlights of the different riveting tests performed. Aspects such as interlock and gap in the interface of the joining sheets were also accounted for the assessment of the connections' quality. Additionally, the mechanical resistance of the joints was tested via tensile-shear, and in some cases three-point bending flexural tests. The results obtained from those destructive tests are the maximum force withstood by the joints and the energy absorbed. These tests allowed making a direct comparison between connections with different characteristics, either rivet geometry or sheet material.

4.1 – Riveting setup and curves analysis

As previously mentioned, the initial tests revealed the need to have a setup adequate to this new T-SPR process applied to butt joints. Three tests were performed using aluminium sheets and stainless-steel rivets with the standard geometry deduced from the applicability window, until having a proper setup. In this section, the results from those tests are presented and analysed.

The first riveted connection was marked by the separation of the sheets during riveting. The setup used consisted of the universal testing machine with the compression plattens attached (Iteration 1). The insertion of the rivet caused the displacement of the sheets moving away from each other on the direction perpendicular to the joint's interface, creating a large gap as visible in Figure 18.

To better understand what was causing the separation of the faying surfaces, the process was analysed step-by-step. The first step of riveting is the clamping of the workpiece and, much like in the SPR processes, it serves to position and secure the sheets in the setup tightly together. In this study, clamping involves the punch lightly touching the rivet before riveting, whilst SPR processes make use of a workpiece holding device, usually called the blank holder.

After clamping, the punch starts pushing the rivet into the workpiece, which is called the indentation stage (stage I). This is a short stage often demarked by a quick rise in load, due to the elastic behaviour of the sheet material. Then, it follows the combined piercing and flaring stage (stage II). This is the largest stage of the process, during which the punch drives the rivet into the workpiece until setting. At this stage, as the rivet is pushed into the workpiece, its skirt deforms outward in the radial direction incited by the angle of the chamfered skirt and the increasing difficulty to penetrate the

gradually more work hardened aluminium sheets. There are no pre-drilled holes, so the rivet transmits the solicitation to the aluminium sheets, displacing material from the workpiece. The skirt's deformation (flaring) soars the radial component of the force transmitted from the rivet to the sheets. Since the friction between the sheets and the bottom platten is insufficient to stop their movement and there is no other force acting in the sheets to counteract that coming from the flaring, during this stage the separation between the sheets increases. In the end of this stage, the rivet is completely set, flush with the sheets' top surface and the punch overcompresses (stage III) the workpiece and rivet. Nevertheless, the overload does not change the thickness of the workpiece, since it is not enough to reach the plastic regime of the sheets, and so it does not contribute to closing the gap. At last, the machine releases the workpiece with negligible elastic recovery of the joint. As mentioned, the result was a separation of the faying surfaces, which was considered unacceptable from a visual and dimensional tolerance standpoint, leading to the modification of the setup.

The second iteration of the setup (Iteration 2) saw the addition of a steel support, over which the workpiece would be placed. The support has a cavity with two margins in the longitudinal direction of the workpiece. In one margin, there are two screws clamping horizontally the sheets against the other margin. The solution helped limiting the movement of the sheets in that direction. However, the high radial forces of flaring, pushing the sheets against the support's margins, originated indentations in the sheet contacting the screws, which in turn, allowed for some unwanted interface gap.

The third iteration (Iteration 3) introduced a steel stop to the support, placed between the screws and the sheet (see Figure 14). The stop diminishes the stress concentrations between the sheet and the screws, further limiting the separation phenomenon.

The different setup tests were performed using identical rivets and sheets. As stated, the rivet's geometry was deduced from the applicability window, above-mentioned in section 2.4. All three connections did not evidence any protrusions or cracks, so the selected rivet was considered appropriate. The riveting parameters used for the setup tests are expressed in Table 2. The diameter, d, chamfer angle, α, and tip width of the rivet, c, are the same for all joints of this study, so it will be implied and not presented on the following tables. The rivet's height is represented by h, and its thickness by t. The workpieces were made of two aluminium sheets, hence the "Al-Al" terminology.

Table 2 – Riveting parameters for the setup tests.

Workpiece	Rivet				
Materials	$h\ [mm]$	$t\ [mm]$	$d\ [mm]$	$\alpha\ [°]$	$c\ [mm]$
Al-Al	4	1.5	10	45	0.2

The changes that the setup introduces to the riveting process parameters are summarized in Table 3, where F_{set} is the force required to set the rivet before overloading, W_{set} is the energy transmitted to the rivet to join the sheets and g is the interface gap. The results of the last iteration showed that it is possible to join two aluminium sheets of $5mm$ thickness in a butt joint with T-SPR

technology, using a stainless-steel rivet. Thus, the setup of Iteration 3 was adopted to proceed with all the subsequent riveting tests of this study's experimental campaign.

Table 3 – Riveting results of the setup tests.

Setup	F_{set} $[kN]$	W_{set} $[J]$	g $[mm]$
Iteration 1 - Without support	37.6	89.3	3.41
Iteration 2 - Support w/ screws	64.0	124.1	0.80
Iteration 3 - Support w/ screws and stop	72.6	131.6	0.33

The results show that the setup effectively reduced the gap between the sheets. Yet, the steel support was not stiff enough to fully eliminate it. The increasingly restrictive setups have a drawback, which is the rise in riveting load and energy spending to rivet identical joints. This translates into a more costly operation due to the greater energy consumption and because it requires machines with higher load capacity. Despite that, the load used to set the rivets falls within the range of loads applied for conventional SPR processes, between $20kN$ and $100kN$ [2]. The support was developed considering the specific plattens and machine used, and is suited for workpieces of approximately $150mm$ length. This means that, to generalize the use of this process to other workpiece geometries, it would be necessary to adopt other solutions for holding the workpieces, such as a blank holder, which could impact the process parameters of force applied, energy consumption and interface gap.

The riveting curves of the three tests are presented in Figure 19 and the respective riveted connections are shown in Figure 20. The fact that the curve respective to the first case of riveting without support (Iteration 1) presents a more accentuated growth of load at the final stage of the curve (overload stage), may be due to the punch compressing the whole workpiece, when the rivet is set. In the other two cases (Iteration 2 and 3), the restriction to the movement of the sheets obliges more material to flow upward inside the rivet's cavity and around the rivet's outer perimeter during piercing. This material is compressed by the punch before it touches the whole workpiece, thus making a more progressive load increase. The difference in the value of displacement which overload starts between Iteration 2 and the other cases is due to tolerances in rivet height from the manufacturing process.

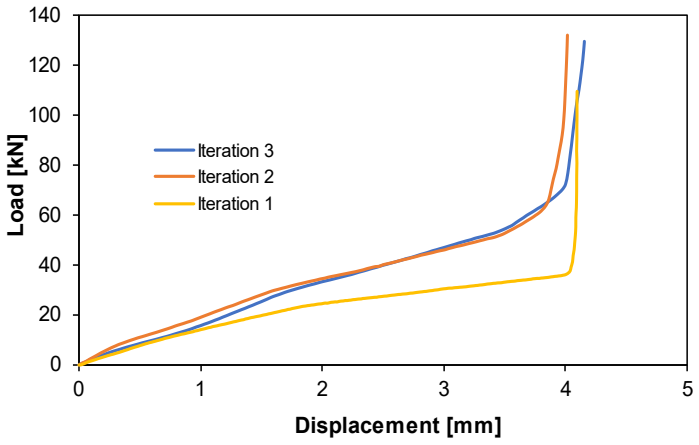

Figure 19 - Riveting curves of the setup tests.

Figure 20 - Riveted sheets with iteration I, II and III
of the setup from top to bottom, respectively.

The results from testing the setup show that the typical riveting curve of T-SPR applied to butt joints presents similarities and some differences to the conventional SPR and DSSPR process curves. The first stage in SPR begins with the rivet forcing the sheets into the die cavity and then piercing through, leading to a steep increase of load, until the whole thickness of the rivet starts piercing the top sheet initiating the second stage. In the present process, the beginning might have a steeper slope until approximately $0.2mm$ of punch displacement (stage I), because the tip is not an edge but rather a flat annular surface with approximately $0.2mm$ thickness. In later experiments, it was seen that some of the curves did not present this feature, instead they started more linearly. That might be explained by the overtightening of the sheets, rising the interface region, thus leaving some space between the sheets and the support's cavity. The curve then resumes with a lower slope, marking the entry to the combined piercing and flaring stage (stage II). It is noticeable two distinct moments during this stage, which are, again, related to the rivet's geometry. The first moment is the initial stretch from the indentation stage up until approximately $1.5mm$, during which the chamfered skirt of the rivet pierces the sheets. The second stretch progresses from that point onward with a flatter slope. During this time, the rivet is piercing the sheets with the portion of the rivet with constant wall thickness, so the load increases at a slower pace. The transition between the first and second moments is very evident and that is because the T-SPR rivet has a sharp transition from the chamfered skirt to the remaining height of the rivet with constant wall thickness. SPR rivets, on the other hand, have a smooth transition between the skirt and the main body, which translates to the riveting curve as a smoother transition as well between these two moments of Stage II.

Even though the projected area of the rivet piercing the sheets is constant during the second moment of the combined piercing and flaring stage, the load keeps swelling due to multiple factors. Among them is the progressive work hardening of the aluminium sheets with the continuous piercing. Another contribution is the friction between the rivet inside the workpiece and the sheets, which increases as more height of the rivet is set. Finally, as the rivet encounters further resistance to piercing, the flaring accentuates, making it more difficult for the rivet to vertically pierce the materials, requiring more load from the machine.

The transition between the stage II and III of the T-SPR curves is sharp. Unlike conventional SPR, in this study, the joints are not overlapped, meaning that there are no vertical gaps between the sheets to close during the compression phase. Because of that, the transition from the rivet setting to overloading of the joint is demarked by a more sudden change in the slope of the riveting curve. The force required to set the rivet corresponds to that point of transition between stage II and III and was named setting load. After overloading, the machine releases the workpiece with negligible elastic recovery of the joint, however, this stage is not shown in the riveting curves.

4.2 – Variation of rivet thickness

In this section, the objective is to understand the impact that the rivet thickness has on the joint's quality and mechanical resistance. The preliminary tests to the setup demonstrated that there are large forces acting on the sheets, pulling them apart, especially towards the end of stage II, for higher levels of rivet flaring. Having this in mind, the thicknesses of the rivets evaluated in this section are all below the $1.5mm$ of the previous connections, as it is expected that thinner rivets require less rivet setting force, thus giving rise to a smaller gap. Therefore, the tests were performed with rivets of $1.25mm$, $1mm$ and $0.75mm$ of thickness, whose results are compared to those of the $1.5mm$ thick rivets. All the rivets have $4mm$ height, riveting aluminium sheets, alike the setup tests. Figure 21 shows the riveting curves respective to each of the rivet thicknesses tested.

The riveting test with the rivet of $0.75mm$ thickness failed due to plastic instability of the rivet. This means that the flaring mechanisms did not occur in the expected way, severely compromising the interlocking and consequently the properties of the joint.

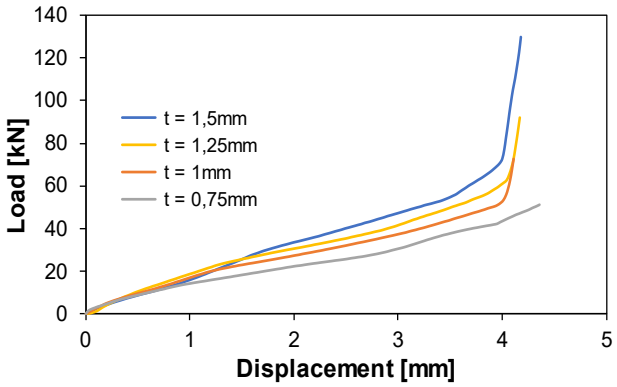

Figure 21 – Riveting curves of the rivet's thickness tests.

From the observation of the curves, one can see that they present a similar slope on the initial riveting stages, until the point where the chamfered section of each rivet is completely inside the materials, with exception of the $t = 0.75mm$ case. From that point on, the curves diverge, as thicker rivets displace more material, demanding more force per unit length of piercing. When reaching the end of stage II, this divergence is intensified, as a thicker rivet wall requires more energy to deform. Finally, the overload stage is demarked by an abrupt rise of load and the curves exhibit an identical slope between each other, again with exception for the case of $t = 0.75mm$.

The values of setting load, energy spent during riveting and the resulting gap of the joints are presented in Table 4. The data shows that riveting with thicker rivets resulted in more gap between the faying surfaces. On the one hand, as thicker rivets displace more material, it is more difficult for the sheet to accommodate the fastener, resulting in a larger gap in the sheets' interface. On the other hand, the punch exerts more force to fasten thicker rivets, that translates into larger radial forces during flaring, which can contribute to the enlargement of the gap.

Table 4 – Riveting results of the rivet thickness tests.

Connection	$F_{set}\ [kN]$	$W_{set}\ [J]$	$g\ [mm]$
$t = 1.5mm$	72.62	131.6	0.58
$t = 1.25mm$	62.62	124.7	0.53
$t = 1mm$	52.05	108.6	0.48
$t = 0.75mm$	42.13	88.7	0.42

The riveted joints of $t = 1.5mm$, $t = 1.25mm$ and $t = 1mm$ were also subjected to tensile-shear tests. The case of $t = 0.75mm$ was not tested, because its connection was not successful. The tensile-shear tests' curves for all the remaining three connections are shown in Figure 22. Table 5 presents the results, where F_{tens} is the maximum force the connection withstood, E_{tens} is the energy absorbed until failure and i is the interlock.

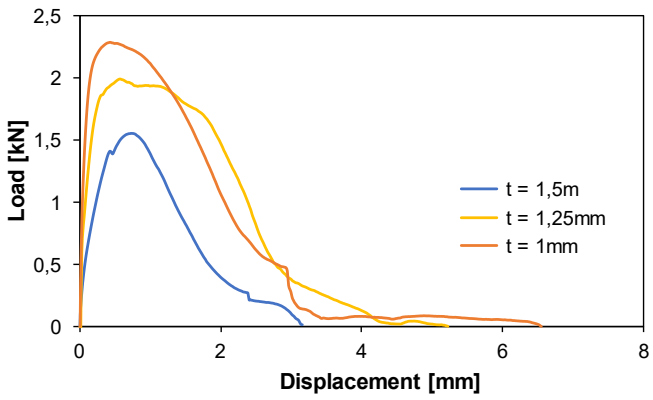

Figure 22 - Tensile-shear tests' curves of joints with different rivet thicknesses.

Similar to the observations of Rita [32] in their experiments with DSSPR, these results show that thinner rivets make the joints resistant to higher tensile-shear loads. Coincidently, the interlock values are larger when using smaller thickness rivets. These observations indicate that, under tensile-shear loading conditions, the dominant factor for the workpiece's strength is the amount of interlock in the joint. The stress state required for plastic deformation is reached with less load, for rivets with thinner a wall section, so a thinner rivet's wall is more easily plastically deformed, guided by the skirt's chamfer. This makes the flaring of the rivet to develop earlier and to a greater extent, enhancing the amount of interlock and ultimately improving the mechanical resistance of the workpiece, assuming that the rivet does not suffer from plastic instability.

Table 5 - Tensile-shear tests' results and mechanical interlocking of joints with different rivet thicknesses.

Connection	F_{tens} $[kN]$	E_{tens} $[J]$	i $[mm]$
$t = 1.5mm$	1.55	2.33	0.76
$t = 1.25mm$	1.99	4.67	0.90
$t = 1mm$	2.29	4.47	1.17

The tensile-shear tests showed a failure mechanism in which the rivet deforms and unfastens itself from the workpiece, as presented in Figure 23. With the tensile load pulling the sheets apart, the sheet's material inside the rivet's hole pulls the rivet in the longitudinal direction of the workpiece (Figure 23c). Because of the flared shape of the rivet, the pulling force is transmitted to it at an angle. That force can be divided into two components, one longitudinal and the other axial (relative to the rivet). The combination of these two components is responsible for making the rivet unfasten. The unfastening takes place as the continuous pulling of the workpiece forces the material originally inside the rivet's cavity to bend towards the back face of the workpiece (circled in green in Figure 23b), while the rivet is forced to bend outward of the workpiece as the reaction (signalled by the angle β in Figure 23c). It was also noted that the sheets bent with the effort from the unfastening, but only a very small amount. The rivet bends until it is completely separated from one of the sheets it is releasing from. From that point onward, as the top sheet continues to be pulled by the testing machine, it slides under the bent rivet, as observable in Figure 23a.

In sum, this failure mechanism is characterized by rendering the joint destroyed, not because the sheets or the rivet fracture but because there is plastic deformation of the rivet and sheets, providing an unfastening mechanism. This failure mechanism explains why the interlock is the dominant factor responsible for the mechanical resistance of the joint, as a more spread skirt will make it more difficult to allow the rivet's release in its axial direction.

(a) Test's direction of pull.

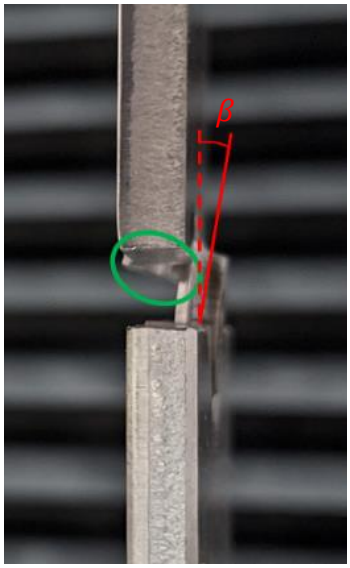

(b) Unfastening's side-view zoomed in.

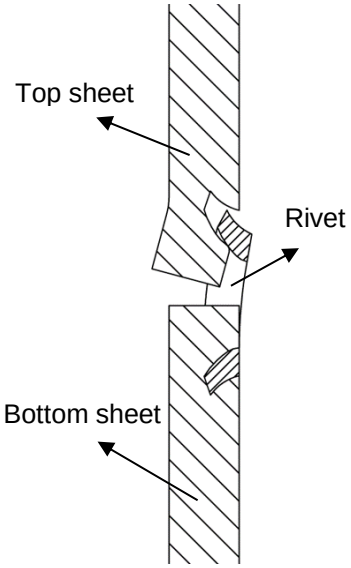

(c) Unfastening section-view illustration.

Figure 23 – Tensile-shear test with the unfastening mechanism between the rivet and the top sheet.

It is also worth noticing that the growth in mechanical interlocking is accompanied by an increasingly smaller growth in the maximum tensile-shear force, because the rivet's capability to resist the failure mechanisms decreases with smaller wall thicknesses. However, with the aluminium sheets and with rivets with height of $4mm$, it was not achieved the tipping point where the wall thickness becomes the dominant factor in tensile-shear resistance. The fact that the energy of rivet $t = 1mm$ is less than that of $t = 1.25mm$ (Table 5) further evidences this trend. The reason for that resides in the fact that, although the interlock helps withstand a larger force, as soon as the rivet is deformed beyond a certain point, the material from the sheet inside the rivet's cavity can more easily bend the rivet with less wall thickness, accelerating the unfastening and making the load decrease more rapidly.

In addition to the tensile-shear tests, the joints of $t = 1.5mm$ and $t = 1mm$ were subjected to three-point bending tests to assess the response of the connections to flexural loading solicitations. There are two different orientations possible for the positioning of the workpieces on the flexural testing setup, and they were both tested. One was named the direct orientation - DO, which the workpiece is placed horizontally in the setup with the visible side of the rivet in the upper face, alike the riveting orientation (Figure 24). The other orientation was named inverse orientation - IO, which consists of positioning the workpiece with the visible side of the rivet facing down (Figure 24).

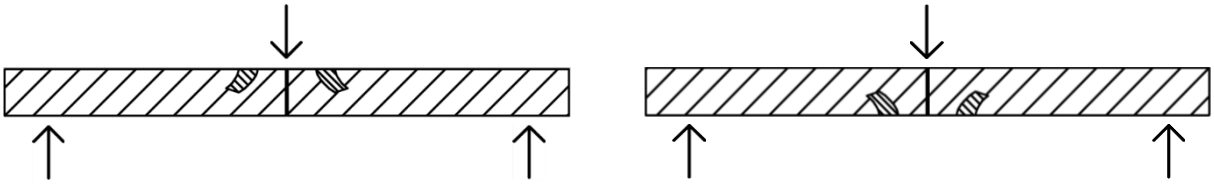

Figure 24 – Illustration of the flexural tests's direct orientation (DO), on the left, and inverse orientation (IO), on the right.

Regardless the orientation, the joints exhibited the same behaviour throughout the tests. As the punch forced the joint downwards, it bent the workpiece. In practice, the sheets remained flat while pivoting around the joint's interface. In the tested cases, the rivet would remain attached to one of the sheets. As the rivet stays attached to one sheet, as the workpiece is bent, it tears the material of the other sheet directly above its flared section.

The curves respective to the flexural tests are presented in Figure 25. They stop at, approximately, a displacement of $10mm$, corresponding to the limit set for punch travel to avoid collisions of the setup. The energy absorbed by the connections was accounted until the end of the curve. The results are shown in Table 6, where F_{bend} is the force applied by the punch, M is the corresponding moment of the force and E_{bend} is the energy absorbed by the joints. With both thicknesses tested, they show that the workpiece is highly sensitive to the direction of the applied moment, as the joints in the DO orientation are much less resistant to flexural loads than those in the IO orientation. The reason for that is the geometry of the rivet's flared skirt. In the DO orientation, the skirt is aligned with the pivoting movement of the sheets as the punch flexures the workpiece, and so the rivet is disassembled more easily from one of the sheets, with less tearing. Despite the ease of disassembly, there is still a progressive tearing of the material above the rivet's skirt from the detaching sheet, starting from the faying surface and progressing along the rivet's perimeter (see Figure 26). In the IO orientation, the skirt is no longer aligned with the pivoting motion of the sheets and the rivet tears the material above its skirt with greater resistance and without the disassembly mechanism, making it more difficult to bend the workpiece.

Table 6 - Three-point bending tests' results.

Connection	$F_{bend}\ [kN]$	$M\ [Nm]$	$E_{bend}\ [J]$
$t = 1.5mm$ DO	0.53	13.2	4.77
$t = 1.5mm$ IO	1.60	40.0	12.94
$t = 1mm$ DO	0.60	15.0	5.74
$t = 1mm$ IO	1.45	36.2	11.69

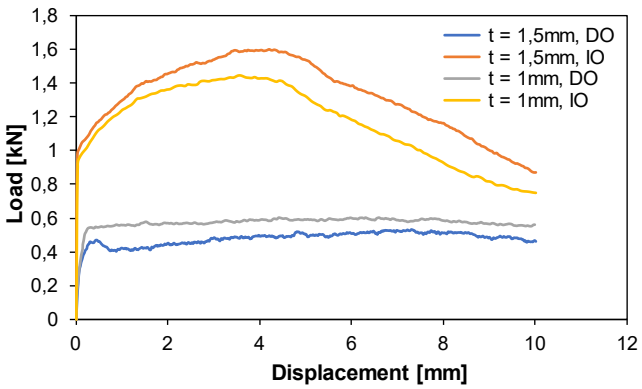

Figure 25 - Three-point bending flexural tests' curves.

The thickness of the rivet impacts the mechanical resistance of the joint to flexural loading in different ways depending on the orientation of the moment. Regarding the case of DO orientation, the thinner wall rivet allows additional load bearing capacity. As seen before, thinner wall rivets provide more interlock. In this case, the additional interlock also helps creating more frictional resistance between the rivet and the sheets. Having more interlock means that the skirt is more spread out, thus less aligned with the disassembly phenomenon, leading to the tearing of more material until failure.

Figure 26 - Close-up view of the teared material from the joint under three-point bending flexural testing, in the DO orientation.

Regarding the IO orientation, the rivet with a thicker wall is advantageous. With this orientation, the failure happens from tearing the detaching sheet, without the drawback of the disassembly mechanism. Thicker rivets pierce deeper into the materials and do not provide so much interlock, but this also means that they have more material to tear under the flexural solicitation. In addition to that, the larger wall thickness makes the rivet more difficult to deform when tearing the material above the skirt.

The results suggest that the greater rivet thickness leads to a greater sensitivity of the joint to the direction of the bending moment solicitation. On the one hand, for the thicker rivet, the unfavourable direction (DO) leads to the lowest resistance. On the other hand, the larger thickness grants the greatest resistance to the joint when solicitated in its favourable direction (IO). Having said this, the selection of the rivet for a given application must consider the applied moment's magnitude and also its direction.

4.3 – Variation of rivet height

The height of the rivet is an important geometrical aspect to consider in riveting processes. Although the rivets used had $4mm$ of initial height, in the end of the process this value is reduced to

about $2.5mm$, for those with $1.5mm$ thickness. So, the sheets are left with a large remaining thickness under the rivet's skirt. Since, the previous joints failed under tensile-shear solicitations due to the deformation of the rivets without the rupture of the sheets, there is room for increasing the rivet height and the piercing depth, by extension. For those reasons, all rivets selected for height testing are taller than the previously tested with $4mm$ height. In this section all joints are aluminium-aluminium using rivets with $1.5mm$ thickness. The selected rivet heights were $4mm$, $4.5mm$, $5mm$, $7mm$ and $10mm$, and their respective riveting curves are shown in Figure 27.

Such as the case of testing with different thicknesses, the riveting curves of the various rivets all begin with an identical slope as the rivet skirt pierces the material. However, in this case the wall thickness of the different rivets is the same, and so the curves are approximately coincident until the point where the whole chamfer has pierced into the sheets. After that, the curves diverge, with taller rivets having lower rates of load increase, as their unfastened section is deformed to a greater extent, and they are more likely to suffer from plastic instability. Finally, the rivet's setting force is larger for taller rivets since there is more material to insert into the sheets, meaning more material gets displaced. The curve respective to the rivet of 10mm height is incomplete, because the rivet suffered from plastic instability, so the discussion of the results is centred on the remaining connections.

Table 7 - Riveting results of the rivet height tests.

Connection	$F_{set}\ [kN]$	$W_{set}\ [J]$	$i\ [mm]$	$g\ [mm]$	$h_{pierce}\ [mm]$
$h = 4mm$	67.36	127.4	0.76	–	2.37
$h = 4.5mm$	77.01	154.9	1.07	0.401	2.50
$h = 5mm$	83.71	186.9	1.19	0.721	2.71
$h = 7mm$	96.60	290.6	1.35	–	3.49

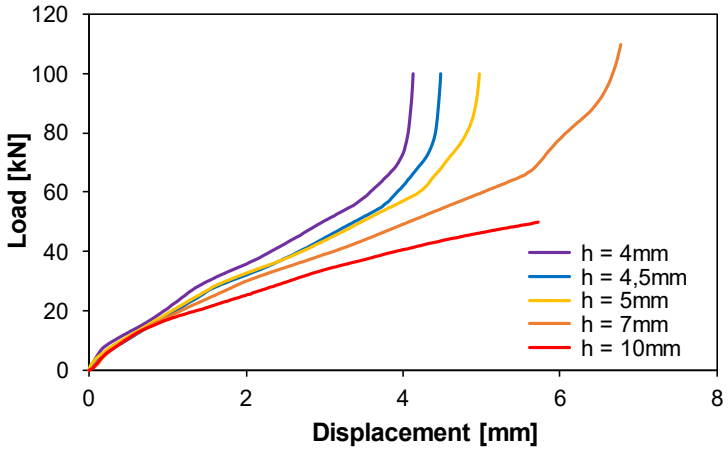

Figure 27 - Riveting curves of the various rivet's height tests.

The results from the riveting tests, including piercing depth, h_{pierce}, are presented in Table 7. They show a trend of interlock increase with the increment of rivet height. As the punch continues to drive the rivet, the chamfer geometry and the work hardening of the sheets encourage the rivet's skirt to flare outward in the radial direction at the same time the piercing depth also grows. Because of that, the increment in rivet height does not translate into an increment of interlock with the same magnitude. Additionally, none of the rivets tested pierced through the sheets or created any protrusions. In sum, with rivets of $1.5mm$ thickness, it was verified that any height increment was transduced into an interlock and piercing depth increment, for any value of height up to the critical height of instability, without causing defects to the joint.

The results also show that the energy spent riveting increases dramatically for taller rivets, which is due to two effects. On the one hand, increasing rivet height means the punch travels a greater distance to set the rivet. Since the area under the riveting curve, which energy relates to, increases at faster pace than the height increment, so does the riveting energy. On the other hand, riveting taller rivets increases the force needed to set, which swells the energetic requirements.

Following the riveting tests, the joints were tested under tensile-shear loading. The resulting curves are displayed in Figure 28 and the results are presented in Table 8. The curves show that the maximum supported load is reached in the early stages of the curve between $0.7mm$ and $1.2mm$ of displacement. The stiffness of the joints is approximately the same, regardless the rivet used, until the point where each joint loses stiffness before reaching the maximum load bearing capacity. This point marks the beginning of the unfastening mechanism where the portion of the rivet fastened to the detaching sheet is gradually bent away from the sheet (see Figure 23). Taller rivets have that point later, since the rivet's flexural resistance increases with the interlock and the piercing depth.

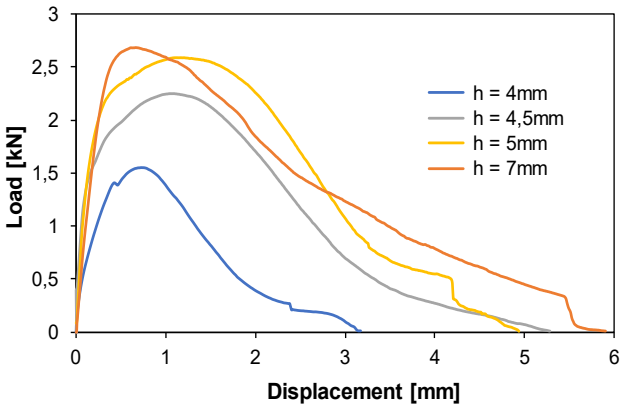

Figure 28 - Tensile-shear tests' curves of connections with different rivet heights.

The results show that the maximum load is greater for taller rivets. They also suggest that the increase of peak load with the rivet height tends to stabilize to a limit of maximum supported load with the $5mm$ thick aluminium sheets used. This behaviour may be explained by two opposing aspects. On the one hand, taller rivets will pierce deeper into the material and obtain a bigger value of interlock,

making it more difficult to unfasten. On the other hand, the increase in piercing depth will decrease the remaining bottom thickness of the material under the rivet skirt.

As depicted in Figure 29a, the material inside the rivet's cavity, is attached to the sheet by the remaining bottom material under the rivet's skirt. That material inside the rivet's cavity is holding the rivet in the tensile-shear tests, making sure it remains attached to the sheet as it is being pulled by the machine. That material then transmits the solicitation to the rest of the sheet through the remaining bottom thickness section, which is the semi-circular section of sheet material under the rivet's skirt with the minimum thickness, leading to a stress concentration. Having less thickness in this region, due to the larger piercing depth, the resisting section is smaller and weaker, ultimately becoming the limiting factor for joint failure. In this way, the joint will fail not because of the unfasten phenomenon, but rather because the resisting section cannot support any more load and is teared by the rivet. To further increase the resistance of the joint, other methods of riveting should be researched. In section 4.5 one of these methods was tested.

Table 8 - Tensile-shear tests' results of connections with different height rivets.

Connection	F_{tens} $[kN]$	E_{tens} $[J]$
$h = 4mm$	1.55	2.33
$h = 4.5mm$	2.25	5.74
$h = 5mm$	2.59	7.24
$h = 7mm$	2.68	7.81

Although none of the connections failed due to sheet material tearing, the case of $h = 7mm$ is close to the point which the sheet's strength becomes the limiting factor. With this rivet, it was observed that the rivet was bent with the tensile load, while bending more significantly the sheet's material inside its cavity. This caused the initiation of tearing by bending of the material in the stress

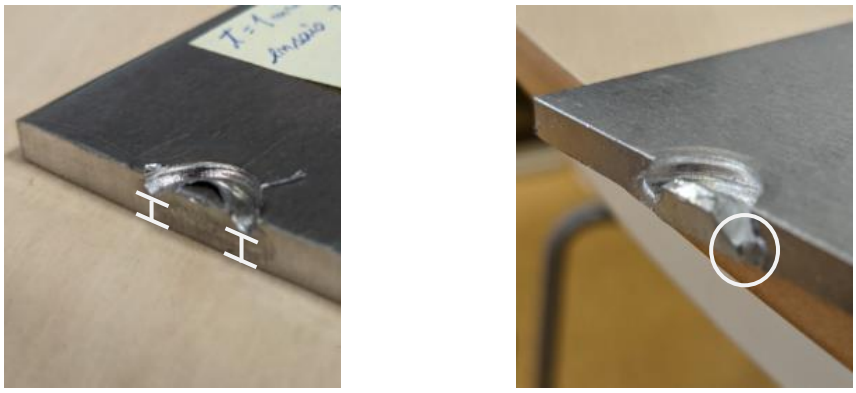

(a) Remaining bottom thickness.

(b) Initiation of tearing of the sheet, signalled by the circle.

Figure 29 - Destroyed joints after tensile-shear testing. Figure at the left, without signs of sheet tearing. Figure at the right with signs of tearing.

concentrated section, under the rivet's skirt, signalled in Figure 29b. This unveils the approximation to a limit where the increase in rivet height can lead to the decrease of the joint's mechanical resistance. However, to fasten thinner rivets it would be necessary a different rivet material, or a softer sheet material.

The interlock is related to the mechanical properties of T-SPR joints, as in SPR joints in general. For DSSPR joints, Alves et al. [21] concluded that the rivet's height has a strong influence in the interlock and, by extension, in the mechanical resistance of the joints. Their conclusion is coherent with these study's results, as taller rivets delivered more interlock in the joints and ultimately increased the capacity of withstanding larger tensile-shear loads. In fact, data shows that the relative increase in resistance of the joint to tensile-shear load (relative to the reference case of $h = 4mm$) follows closely the relative increase of the interlock value. Figure 30 denotes this relation with the nondimensionalized values of tensile-shear load and interlock, for the tested rivet heights, as the ratio between the respective joint's value of maximum tensile force or interlock, and the analogous value of the $h = 4mm$ case. It is also worth noting that, as the rivets are taller, the increase in height results in an increasingly smaller increment of interlock, as previously discussed.

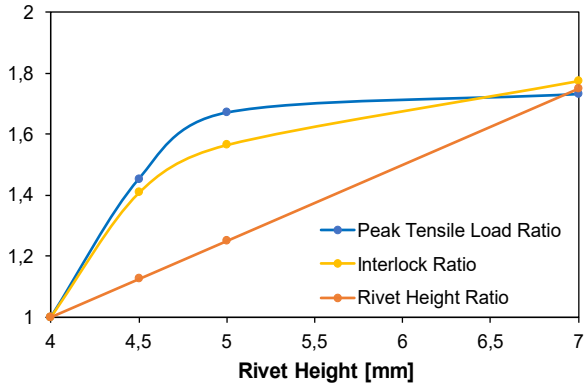

Figure 30 - Non-dimensionalized tendencies of rivet height, interlock and maximum tensile load.

Regarding the tests to different thicknesses and the latest with different heights, one can conclude that riveting with a smaller or a larger rivet comes down to a balance that one needs to ponder. Riveting with smaller rivets requires less energy and because they take less load to fasten, the machines used may be less robust and cheaper. However, the riveting of larger rivets means a smaller number of rivets to fasten in a multi-riveted joint to achieve the same properties, meaning less cycle times. The trends observed are that, among the tested rivet dimensions, thinner and taller rivets provide the most resistance to tensile-shear loading conditions for joints made of $5mm$ thick aluminium sheets. Thinner rivets provide the added benefit of a lighter joint. From the bending tests it was observed that thicker rivets provide the most and the least resistance to the joint depending on the direction of the applied moment. However, more testing should be conducted to take more grounded conclusions about this loading scenario.

4.4 – Workpiece's material joinability

In this section, the objective is to test the ability to join different materials with one type of rivet, both in similar and dissimilar connections. The rivets used were all identical, made of stainless-steel as in the previous joints, with the standard dimensions deduced from the applicability window (see Table 2). The workpieces tested were aluminium-copper (Al-Cu), copper-copper (Cu-Cu) and PVC-PVC.

The riveting results of those workpieces and the previously riveted aluminium-aluminium (Al-Al) are shown in Table 9. Figure 31 presents the riveting curves of the metallic workpieces. None of the tested joints presented any protrusions or cracks. From the data, it is evident that the Cu-Cu connection implies more applied load and energy spending throughout the riveting process. That is because the copper has greater mechanical resistance and is a harder material compared with the aluminium alloy used. Even though the joining of the copper sheets required more force, the rivet did not unstabilize. Additionally, the data shows that the gap between the faying surfaces increases from the Al-Al connection to the Al-Cu, and from the latter to the Cu-Cu. The aluminium-copper riveting curve is positioned between the curves of the similar connections of the two materials, as expected, since the global properties of the workpiece are average between the Al-Al and Cu-Cu (see Figure 31). In any case, the three curves present the same stages of the reference riveting curve.

Table 9 - Riveting tests' results of different workpiece materials combinations.

Connection	F_{set} $[kN]$	W_{set} $[J]$	g $[mm]$
Al-Al	72.62	131.6	0.33
Al-Cu	78.73	148.8	0.61
Cu-Cu	92.69	17.8	0.69
PVC-PVC[1]	17.74	31.3	–

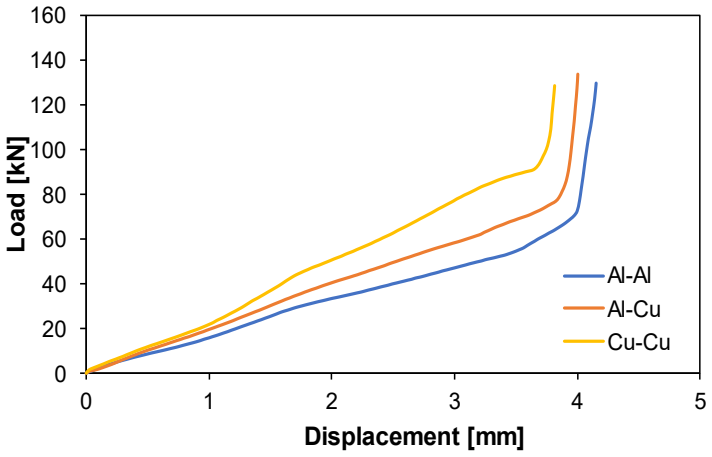

Figure 31 - Riveting curves of the Al-Al, Al-Cu and Cu-Cu joints.

[1] The PVC joint was made with a rivet having $1mm$ wall thickness, whilst the remaining have $1.5mm$

The riveting of PVC-PVC joints presented a distinct challenge. With the current setup, the sheets buckled during piercing. As a result, when the punch released the workpiece, the elastic recovery of the joint returned it to an arched shape with a large interface gap, as shown in Figure 32, despite the punch had flattened the sheets during the rivet setting.

Even though the tested combination of rivet and sheets had been used successfully in other experiments, for instance with DSSPR technique [28] and $8mm$ high rivets, in this case it was not possible. With all the similarities between DSSPR and T-SPR, the immediate hypothesis to the cause of the buckling is the setup, with the sheets being too compressed by the stop in the support. With that in mind, a new joint was riveted, this time with minimum tightening of the stop against the sheets. The results revealed the same behaviour as before, even though the deformation of the workpiece was slightly reduced. The piercing and flaring phases of the process tend to push the two sheets apart in the longitudinal direction, giving rise to a compressive force against the support's boundaries above the critical buckling load. The deformation of the sheets with the rising up of the interface region, with a shape similar to the first buckling mode of a beam, is explained by the high friction forces between the boundaries of the workpiece and the support, and the impossibility of the material to push down the support cavity where it rests.

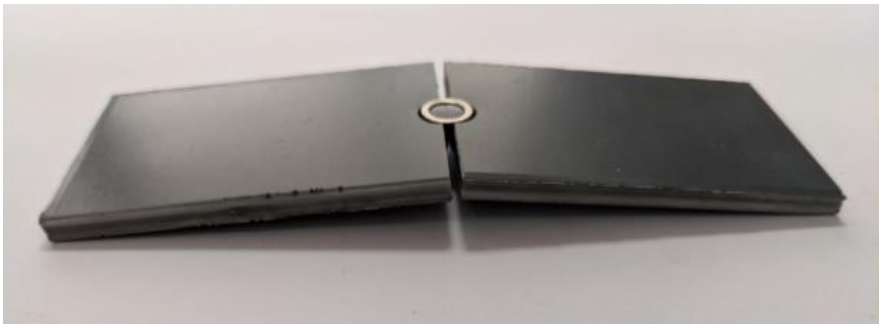

Figure 32 – PVC-PVC joint, riveted with standard rivet.

Considering the experimentation done with rivets of different thicknesses, in section 4.2, it was decided to rivet new sheets with a rivet of $1mm$ thickness instead of the previous $1.5mm$, adding less volume to the joint. The results were the mitigation of the arched shape after the elastic recovery and less interface gap, as observed when riveting aluminium sheets. Nevertheless, the gap is still much larger than that observed in the Al-Al connections. From these results, one may conclude that the current support is not well suited for joining PVC sheets. It would be interesting to analyse whether a machine equipped with a blank holder would enable the production of PVC-PVC connections of higher quality.

The riveting curves of PVC-PVC and Al-Al riveted with rivets of $t = 1mm$ are shown in Figure 33. As seen before when joining copper, the material has a major influence on the riveting curve. In this case, having much lower mechanical resistance, the PVC requires smaller values of force and energy to set the rivet. The PVC-PVC curve presents the same stages as the analogous Al-Al curve,

however with reduced magnitude of load. None of the joints tested in this section showed any sign of protrusions.

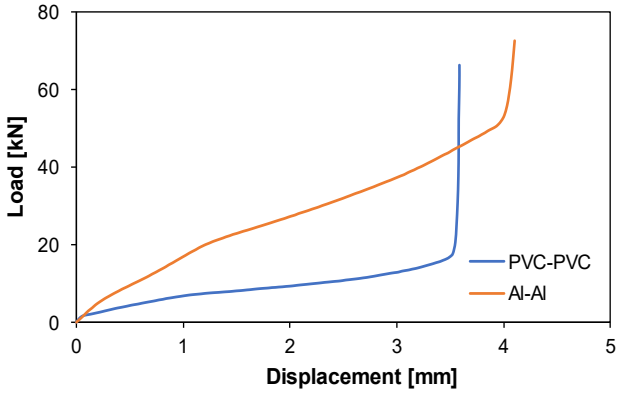

Figure 33 - Riveting curves of the PVC-PVC and Al-Al joints with $t = 1mm$ rivets.

In sum, with these experiments it was not proven that one can rivet workpieces with widely different material properties, however that ability depends on setup, rivet geometry and how broad is the range of properties. Rivets with $h = 4mm$ and $t = 1.5mm$ were successfully used to join Al-Al, Al-Cu and Cu-Cu workpieces. Rivets with the same height and $t = 1mm$ were able to produce connections of Al-Al and PVC-PVC workpieces.

Often the hardness of the rivet is tailored according to the hardness of the workpieces, even so, as shown here it is possible to join a wide range of materials using a same rivet material, as long as it is sufficiently harder than the workpieces. This is something that can be observed also in the industry. For instance, Böllhoff claims that its HDZ type rivet is able to join materials in the range of tensile strength from less than $400MPa$ (some 5000s aluminium alloys) up to $1600MPa$ (press-hardened steels), without changing the rivet's geometry and material [24]. Having one rivet able to fasten various materials, might bring benefits in storage and logistics costs, as well as in production cycle times and error minimization.

4.5 – Riveting method for improved mechanical resistance

From the observations of the failure mechanisms of the joints in sections 4.2 and 4.3, it was noted a slight bending of the sheets during tensile-shear testing. The bending tends to align the rivet's movement of unfastening with the loading direction, allowing the rivet to more easily release from the top sheet. This causes a reduction of the maximum load that the joint can withstand.

One possible solution to this problem is the insertion of an extra rivet in the joint, on the opposite side of the first. With this, it is expected that the unfastening mechanism of both rivets creates bending in opposite directions, cancelling each other out. This method was put to test using two identical rivets with the standard dimensions of $h = 4mm$ and $t = 1.5mm$. First was the setting of rivet A, named this way for distinction purposes, and then the workpiece was flipped with the upside down and rivet B was inserted, using the same setup as for the previous connections. The curves and results of the two rivets' fastening are presented in Figure 34 and Table 10, respectively. The first rivet shows the expected curve for the type of rivet used, with the value of setting force and energy similar to those obtained before in tests with an identical rivet. As the second rivet is inserted, it faces already work hardened material, which makes piercing more difficult and so the skirt flares outward to a greater extent. Furthermore, because the rivets are fastened coaxially, rivet A presents an obstacle to the insertion of rivet B and the movement of dislocations inside the sheet, obstructing the piercing of rivet B and promoting the flaring of its skirt. The curve respective to rivet B demonstrates these two contributions, having a steeper slope through the entire process. The curve appears unfinished, because it was used a load limit of $100kN$ for the rivet, which limited the setting of that rivet prematurely.

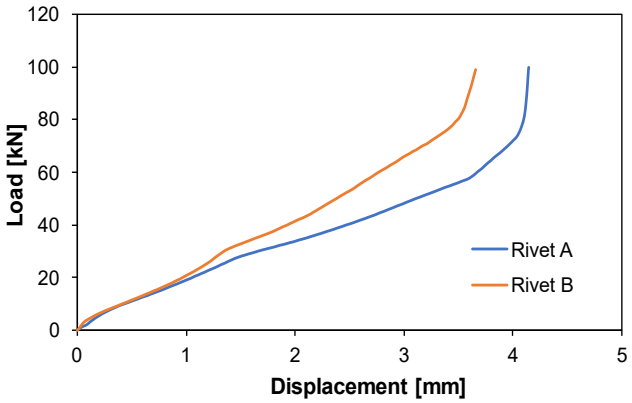

Figure 34 - Riveting curves of the double riveted connection.

Even though, the joint has two rivets instead of one, the interface gap was kept constant at $1.3mm$ before and after setting rivet B. However, the additional rivet made the expansion, in the width direction, of the material at the interface increase from $0{,}7mm$ with a single rivet, to $1.4mm$ with two rivets. The expansion is greatest in the plane of interface of the sheets and reduces for sections further away from the rivet until the face of contact with the support, which has no variation in width. The values of width expansion at the interface evoke the need to test this joining technique in different configurations for multi-riveted applications, considering aspects such as the gap in the interface and the dimensional variation of the sheets.

Table 10 – Results of riveting the double riveted connection.

Connection	$F_{set}\ [kN]$	$W_{set}\ [J]$	$i\ [mm]$
Rivet A	73.56	140.6	0.96
Rivet B	100.0	150.5	1.19

The results also show that it is important to keep in mind the different load magnitude requirements when joining two coaxially fastened rivets, as the setting force increases for the second rivet. Additionally, this method also contributes to a larger interlock for the second rivet, which throughout this study was found to be an important feature to achieve a stronger connection.

The joint was then subjected to a tensile-shear test. The test's curve is shown in Figure 35 and the results in Table 11, overlapped with curves and results, respectively, of previous joints. The tensile-shear curve in this case is different than the previous. The failure of the joint was attributed to the failure of the top sheet. As expected, the rivets cancelled each other's contribution to the bending of the sheet and remained attached to both sheets until the fracture of the top sheet (Figure 36). The contribution of both rivets allowed the resistance of more than triple the load that a joint with a single rivet, identical to the latter, withstands. These results also show that riveting with smaller rivets can be more energy efficient. The sum of the riveting energy of both $h = 4mm$ rivets is approximately the same than that used for riveting one single $h = 7mm$ rivet ($290.6\ J$). However, with two rivets the joint's resistance to tensile-shear loading is greater than having a one $h = 7mm$ rivet.

Table 11 - Tensile-shear tests' results of the connection with two standard rivets, single standard rivet and single $h = 7mm$ rivet.

Connection	$F_{tens}\ [kN]$	$W_{tens}\ [J]$
Two rivets	4.89	1.59
$h = 4mm$	1.55	2.33
$h = 7mm$	2.68	7.81

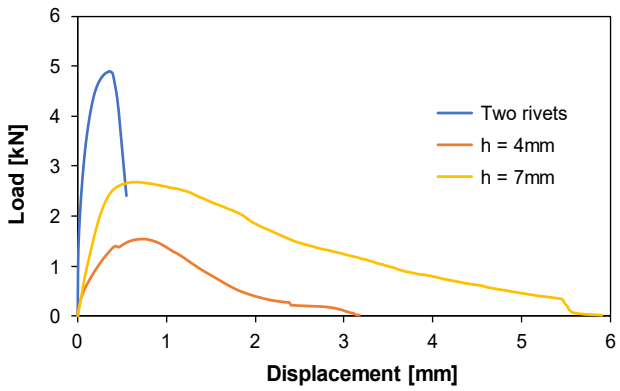

Figure 35 - Tensile-shear tests' curves of the connection with two standard rivets, single standard rivet and single $h = 7mm$ rivet.

As expected, the joint failed in the section where the remaining bottom thickness is minimum, as the stress concentrations are higher as shown Figure 36. In the previous connections it was seen that the bottom material thickness was not a limiting factor for the resistance of the joint riveted with the T-SPR technique. However, with this experiment it was observed that if a configuration of two coaxial rivets is implemented, the thickness of material in between the rivets will dictate the failure mode and mechanical properties of the connection.

Despite achieving a higher tensile load, the joint absorbed significantly less energy before failure, because it did not have the failure mechanisms of the other joints, such as the unfastening, that reduced the maximum load but allowed the workpiece to absorb more energy.

This riveting configuration was not subjected to flexural testing, but the difference in the interlock between the two rivets suggests that the response to such solicitation would vary, to some extent, depending on the direction of the applied moment, as observed before in joints with a single rivet.

This method of joining with two rivets could be an alternative to DSSPR when, for practical reasons, it is not possible to position the DSSPR rivet between the joining sheets. However, the joint will not have the same resistance to shear conditions. Having riveted the same aluminium alloy sheets of $t = 5mm$, Alves et al. [21] achieved a maximum shear strength of $11.5kN$ with a DSSPR rivet identical to those used in this study but with $8mm$ height, whilst the technique of T-SPR applied to butt joints reached a strength of $1.55kN$ with a single rivet and $4.89kN$ with two rivets of $h = 4mm$.

Figure 36 – Rivets attached to the top sheet after rupture of the bottom sheet in double riveted connection.

Chapter 5

Conclusions

5.1 – Achievements and conclusions

The objective of this work was to experiment the potential and the applicability of the T-SPR process to the joining of sheets in a butt configuration, without auxiliary straps, and using a flat die. In total, the experimentation spread into five separate subjects mentioned below. All the considerations here taken are only valid considering the whole of the tests' conditions, which includes the setup, the rivet's material and geometry and the sheets' dimensions and materials.

The first test revealed the need to use a setup that would keep the aluminium sheets together during riveting. To be able to do so, it was first developed the setup that would yield quality joints. The final iteration of the setup consisted on the machine, two plattens and a flat support with two margins, in the longitudinal direction, a steel stop and two screws, making it adjustable to slight variations in length between the different workpieces. With this setup, it was shown that it is possible to join two aluminium sheets of 5mm thickness with T-SPR technology in a butt joint configuration, using tubular rivets and a flat die.

The second path was to test the influence of the rivet's thickness in joints of two aluminium sheets. It was observed that using rivets with less thickness it is required less setting force and energy for the riveting of the connections, and so it is possible to make the operation less costly and use machines that are less robust. The gap between the faying surfaces was also reduced for thinner rivets. The resistance to tensile-shear loading is improved for thinner rivets, because of the increase in interlock they provide. The various tensile-shear tests showed a failure mechanism, characteristic of this process applied to butt joints, that involves the unfastening of the rivet, through the bending of the fastener and the sheet material residing inside the rivet's hole. Among the thicknesses tested, the maximum tensile-shear load achieved was $2.29kN$, with an interlock of $1.17mm$, using a rivet of $t = 1mm$. This connection had a gap of $0.48mm$ and absorbed $4.47J$ of energy. Despite being the most resistant joint, it did not present the most energy absorption among the tested connections.

The third object of analysis was the contribution of different rivet heights to the resistance of the connections. It was observed that both the interlock and the piercing depth increased with the increase in rivet height. Additionally, because of the failure mechanisms, it was observed a close relation between the growth of interlock and the rise in tensile-shear resistance of the joint. Riveting with taller rivets provides stronger joints but demands more force from the machine and especially more energy, due to the increase in applied force in conjunction with the longer punch travel. Neither the joint riveted with a rivet of $h = 7mm$, or any of the others, showed signs of protrusions or cracks in the sheets. It was seen that the increase in rivet height translates into a stronger joint to tensile-shear conditions only until a limit, for two reasons. One is the limit to how tall the rivet can be, as it suffers

from plastic unstability, if taller than the critical height of unstability. The other limit is the mechanical resistance of the sheets, because taller rivets reduce the section of the sheet material resisting the solicitation, making the material more prone to tearing in the destructive test. Despite all rivets have unfastened before sheet rupture, a different combination of rivet material and sheet material can change that failure mechanism

The inferred standard rivet geometry from the applicability window, suggested by Rita [32] for DSSPR joints, was adequate for joining aluminium specimens. Yet, from the tested joints, the connection of $h = 7mm$ and $t = 1.5mm$ was the most resistant to tensile-shear loads, holding $2.68kN$ and absorbing $7.81J$, against $1.55kN$ and $2.31J$ of the standard rivet. From the experimentation, it can be inferred that the combination of a long and thin rivet favours the strength in tensile-shear loading.

The fourth subject was related to testing the ability of one rivet geometry, in this case, the standard of $h = 4mm$ and $t = 1.5mm$, to join workpieces of materials with widely different mechanical properties. As one could expect, it is necessary to use more force and energy to rivet workpieces constituted by materials with superior mechanical resistance. So, the joining of the Cu-Cu workpiece took the most amount of force and energy, since copper has greater mechanical resistance, followed by the Al-Cu, Al-Al and PVC-PVC joints, in that order respectively. The riveting of the workpieces was successful in the sense that none of the connections exhibited signs of protrusion or cracks. However, the riveting of the PVC-PVC workpiece with the standard rivet was deemed unfeasible, with the buckling of the sheets during piercing. The joining of PVC sheets indicated that the setup should provide the workpiece with vertical clamping force during riveting, to avoid buckling. In any case, it was possible to join the PVC sheets using a thinner rivet of $t = 1mm$, which is the rivet geometry providing the best performance in the thickness tests to Al-Al joints. Having said this, it was not found a rivet to join workpieces from Cu-Cu to PVC-PVC, nevertheless, there is still a wide range of materials that one rivet type may fasten.

The fifth experimental subject was a method that would provide better results to tensile-shear solicitations. It consisted in riveting both sides of the Al-Al workpiece with two standard rivets coaxially positioned. The insertion of the second rivet required higher force and energy but also granted a higher value of interlock than the first rivet. The tensile-shear test showed that the two coaxial rivets changed the failure mechanism from unfastening of the rivet to rupture of the sheet, without unfastening. With this method of two coaxial rivets, the joint reached a tensile-shear load of $4.89kN$, instead of the previous $1.55kN$ with a single rivet, which is more than triple the resistance while using double the amount of rivets. In a multi-riveted workpiece, this might be a solution to ponder.

The flexural tests showed a large dependency of the joints' flexural resistance on the direction of the applied moment. It was seen that this dependency was aggravated if using a thicker rivet. However, the number of tests was very small and so these conclusions are only valid for the cases of rivets with $h = 4mm$ and $t = 1mm$ and $t = 1.5mm$. The stronger connection was that with the thicker rivet withstanding a maximum moment of $40Nm$ in the solicitation direction named IO.

It can be stated that in all tests, except for the coaxial rivets, the interlock was of utmost importance regarding the resistance to tensile-shear loading conditions. Nevertheless, it was observed a trend of stabilization of the mechanical resistance achieved by the joints, for instances when the rivet wall thickness or the sheets' remaining bottom thickness are too small.

With this process, sheets were joined using flat tools and rivets of simple geometry. This technique has its own disadvantages. For instance, even though the die is flat, the process needs some means of securing the workpiece in the direction perpendicular to the sheets' interface plane, which are subjected to high separation forces. Additionally, this technology does not provide hermetic or water-tight seals because of the gap created during the riveting. Finally, in what concerns the visual aspect, unlike SPR, the joint of T-SPR does not show protrusion. However it leaves one side of the rivet visible, unlike DSSPR for which the fastener is hidden inside the joining materials.

5.2 – Future work

This process was mostly characterised by riveting results and the mechanical resistance of the connections in tensile-shear loading conditions. The next steps could be the testing of T-SPR butt joints with other loading scenarios such as shear or torsion, and with fatigue solicitations. Despite having conducted flexural tests, those were very few so one might suggest a more thorough testing of the joints under flexural solicitation. Concerning the process, hybrid rivet bonding is yet to be tested with butt joints. This could impact the strength and failure behaviour of the rivet-bonded joint, and take this riveting process to new applications.

As visible by the colour of the rivets (see Figure 13), they undergo though a thermal cycle while being machined. This may be equivalent to a heat treatment that can affect the rivets' material properties. It would be interesting to evaluate the influence of the production process of the rivets can have on the results.

It was not found a common rivet to join materials from Cu-Cu to PVC-PVC, however, there are promising rivets that could make it possible that were not tested, for instance the fastening of copper sheets with a rivet of $h = 4mm$ and $t = 1mm$. Additionally, the PVC-PVC joints should be further tested using a different setup that prevents the sheets from buckling, for instance, one of conventional SPR with a blank holding device. Still regarding the setup, it would be interesting to join the sheets with an improved version of the latter, or experiment with a different setup featuring a v-ring indenter, for instance, that would offer a solution for further minimising the gap created during the riveting. At last, the use of flat tools can bring interesting results when riveting less ductile materials, and so a possible track for future work could be to explore how wide is the range of joinable materials using T-SPR technology with such tools, regarding aspects such as workpiece ductility.

One last aspect worth researching is how different riveting configurations of multi-riveted butt-joints can impact the mechanical resistance of the connections, following the test of coaxially opposed rivets. Different rivet geometries and positioning configurations, for instance giving an offset to the

rivets' axis instead of being coaxially opposed, can benefit the joint's mechanical resistance. Additionally, the conjugation of multi-riveted configurations with single tall rivets, in the same workpiece, might bring broader mechanical resistance to the connection, with high tensile load resistance, from the multi-riveted configuration, and high energy absorption, from the tall rivet.

The results from this study set an experimental foundation that can be used as a reference for the future development of models for computational simulations using finite element methods, for the testing of different rivet and sheet combinations, with varying geometries and materials more efficiently. Computational simulations could also allow to more accurately associate the material flow and deformations occurring in the joint to each point of the respective physical riveting curve. Additionally, these simulations could help predict the failure mechanisms for each workpiece and rivet combination. It would be interesting to find ways of mitigating the interface gap and improving the joints' mechanical resistance using these types of simulations.

Bibliography

[1] Collette, Quentin & Wouters, Ine & Leen, Lauriks (2011). Evolution of historical riveted connections: joining typologies, installation techniques and calculation methods. *WIT Transactions on the Built Environment, 118*. doi: 10.2495/STR110251.

[2] Li, Dezhi & Chrysanthou, A. & Patel, Imran & Williams, Geraint. (2017). Self-piercing riveting-a review. *The International Journal of Advanced Manufacturing Technology, 92*, 1777–1824. doi: 10.1007/s00170-017-0156-x.

[3] Böllhoff website, RIVSET® Automation E, *RIVSET® Automation E – When modern multi-material designs electrify (divc94363c9dd.cloudfront.net), accessed 3 April 2023.

[4] Atlas Copco website, https://www.atlascopco.com/pt-pt/itba/industry-solutions/automotive-entry/self-pierce-riveting, accessed 5 April 2023.

[5] Ang, H.Q. (2021). An Overview of Self-piercing Riveting Process with Focus on Joint Failures, Corrosion Issues and Optimisation Techniques. *Chinese Journal of Mechanical Engineering, 34*. doi: 10.1186/s10033-020-00526-3.

[6] He, X., Wang, Y., Lu, Y. et al. (2015). Self-piercing riveting of similar and dissimilar titanium sheet materials. *The International Journal of Advanced Manufacturing Technology, 80*, 2105–2115. doi:10.1007/s00170-015-7174-3.

[7] S. Chen, D. Jin, H. He, F. Yang and J. Yang, (2022). Deep Learning Based Online Non-Destructive Defect Detection for Self Piercing Riveted Joints in Automotive Body Manufacturing. *IEEE Transactions on Industrial Informatics*. doi: 10.1109/TII.2022.3226246.

[8] Neuser, Moritz & Kappe, Fabian & Busch, M & Grydin, Olexandr & Bobbert, Mathias & Schaper, Mirko & Meschut, G & Hausotte, T. (2021). Joining suitability of cast aluminium for self-piercing riveting. *IOP Conference Series: Materials Science and Engineering, 1157*. doi: 10.1088/1757-899X/1157/1/012005.

[9] P. Johnson, J.D. Cullen, L. Sharples, A. Shaw, A.I. Al-Shamma'a. (2009). Online visual measurement of self-pierce riveting systems to help determine the quality of the mechanical interlock. *Measurement, 42*, 661-667. doi: 10.1016/j.measurement.2008.10.013.

[10] Wayne Cai, P.C. Wang, Wu Yang (2005). Assembly dimensional prediction for self-piercing riveted aluminum panels. *International Journal of Machine Tools and Manufacture, 45*, *6*, 695-704. doi: 10.1016/j.ijmachtools.2004.09.023.

[11] Aslan, F., Langlois, L. & Balan, T. (2019). Experimental analysis of the flow drill screw driving process. *The International Journal of Advanced Manufacturing Technology, 104*, 2377–2388. doi: 10.1007/s00170-019-04097-z.

[12] Website from Böllhoff, RIVTAC® high-speed joining | Böllhoff (boellhoff.com), accessed 11 April 2023

[13] Stephan Altvater, Sebastian P. Sikora, Tjark Siefkes, (2022). Transition between flow-drill screwing systems considering joining process and joint characteristics. *Advances in Industrial and Manufacturing Engineering, 5*. doi: 10.1016/j.aime.2022.100091.

[14] Kascak, Lubos & Spišák, Emil & Mucha, Jacek. (2012). Evaluation of properties of joints made by clinching and self-piercing riveting methods. *Acta Metallurgica Slovaca. 18*, 172-180.

[15] Xiaoqiang Ren, Chao Chen, (2022). Research on a single-point butt clinching process with various forming forces. *CIRP Journal of Manufacturing Science and Technology, 39*, 308-316. doi: 10.1016/j.cirpj.2022.08.013.

[16] Manladan, S.M., Yusof, F., Ramesh, S. et al. (2016). A review on resistance spot welding of magnesium alloys. *The International Journal of Advanced Manufacturing Technology 86*, 1805–1825. doi: 10.1007/s00170-015-8258-9.

[17] Zhang H, Senkara J (2011) Resistance welding: fundamentals and applications. CRC Press, Boca Raton (cited in [16]).

[18] Wu, J., Chen, C., Ouyang, Y. et al. (2021). Recent development of the novel riveting processes. *International Journal of Advanced Manufacturing Technology 117*, 19–47. doi: 10.1007/s00170-021-07689-w.

[19] Meschut, G., Janzen, V. & Olfermann, (2014). Innovative and Highly Productive Joining Technologies for Multi-Material Lightweight Car Body Structures. *Journal of Materials Engineering and Performance, 23*, 1515–1523. doi: 10.1007/s11665-014-0962-3.

[20] Han, L. & Thornton, M & Shergold, Mike. (2023). A comparative study between self-piercing riveting and resistance spot welding of aluminium sheets for the automotive industry.

[21] Alves, L.M., Afonso, R.M. & Martins, P.A.F., (2020). Double-sided self-pierce riveting. *The International Journal of Advanced Manufacturing Technology, 108*, 1541–1549. doi: 10.1007/s00170-020-05503-7.

[22] Y. Durandet, R. Deam, A. Beer, W. Song, S. Blacket, (2010). Laser assisted self-pierce riveting of AZ31 magnesium alloy strips. *Materials & Design, 31*, S13-S16. doi: 10.1016/j.matdes.2009.10.038.

[23] Li, Yongbing & Wei, ZeYu & Wang, Jiao & Li, YaTing. (2013). Friction Self-Piercing Riveting of Aluminum Alloy AA6061-T6 to Magnesium Alloy AZ31B. *Journal of Manufacturing Science and Engineering, 135*. doi: 10.1115/1.4025421.

[24] Böllhoff, HDZ rivet joinable materials. https://www.boellhoff.com/de-en/products/additional-product-ranges/rivset-self-pierce-riveting-technology/#c378, accessed 15 April 2023.

[25] Zhenghua Rao, Liang Ou, Yaqiong Wang, Pei-Chung Wang. (2020). A self-piercing-through riveting method for joining of discontinuous carbon fiber reinforced nylon 6 composite. *Composite Structures, 237*. doi: 10.1016/j.compstruct.2019.111841.

[26] Liu, Y., Wang, G., and Weiler, J., (2023). Padded Self-Piercing Riveting (P-SPR) on Magnesium High Pressure Die Casting. *SAE International Journal of Advances and Current Practices in Mobility, 5*. doi: 10.4271/2022-01-0249.

[27] N.-H. Hoang, R. Porcaro, M. Langseth, A.-G. Hanssen, (2010). Self-piercing riveting connections using aluminium rivets. *International Journal of Solids and Structures, 47, 3 - 4,* 427-439. doi: 10.1016/j.ijsolstr.2009.10.009.

[28] L.M. Alves, R.M. Afonso, P.A.F Martins, (2021). Double-sided self-pierce riveting of polymer sheets. *Journal of Advanced Joining Processes, 3*. doi: 10.1016/j.jajp.2021.100051.

[29] Alves, L.M., Afonso, R.M., Pereira, P.T. et al., (2021) Double-sided self-pierce riveting of dissimilar materials. *The International Journal of Advanced Manufacturing Technology, 115*, 3679–3687. doi: 10.1007/s00170-021-07426-3.

[30] K. Kato, M. Okamoto, T. Yasuhara, (2001). Method of joining sheets by using new type rivets. *Journal of Materials Processing Technology, 111*, 198-203. doi: 10.1016/S0924-0136(01)00519-2.

[31] Huang, Zhichao & Yao, Qiuhua & Lai, Jiamei & Zhao, Jingwei, (2017). Developing a self-piercing riveting with flange pipe rivet joining aluminum sheets. *The International Journal of Advanced Manufacturing Technology, 91*, 2315–2328. doi: 10.1007/s00170-016-9938-9.

[32] Afonso R.M., Rita R.M., (2021). Rebitagem auto-perfurante de dupla face aplicada a chapas de espessura fina. MSc Thesis in Mechanical Engineering, Instituto Superior Técnico, Universidade de Lisboa.

[33] Md Abdul Karim, Taek-Eon Jeong, Wooram Noh, Keun-Young Park, Dong-Hyuck Kam, Cheolhee Kim, Dae-Geun Nam, Hudson Jung, Yeong-Do Park, (2020). Joint quality of self-piercing riveting (SPR) and mechanical behavior under the frictional effect of various rivet coatings. *Journal of Manufacturing Processes, 58,* 466-477. doi: 10.1016/j.jmapro.2020.08.038.

[34] A new rivet that enables consistent joint quality in multiple layers of high-strength aluminum. Website from Henrob, https://www.atlascopco.com/content/dam/atlas-copco/industrial-technique/general/documents/brochures-leaflets/joining-solutions/t-rivet-pdf.pdf, accessed 17 April 2023.

[35] B Çevik, B Gülenç, (2018) The effect of welding speed on mechanical and microstructural properties of 5754 Al (AlMg3) alloy joined by laser welding. *Materials Research Express, 5*. doi: 10.1088/2053-1591/aad3b0.

[36] Thyssenkrupp's website, https://www.thyssenkrupp-materials.co.uk/aluminium-5754.html, accessed 9 May 2023.

[37] MatWeb's website, https://www.matweb.com/search/DataSheet.aspx?MatGUID=25cdd9bd3ebb4941be91cb0bee4cc661, accessed 10 May 2023

[38] Intek Plastics, Inc. website, https://www.intekplastics.com/materials-guide/rigid-pvc/, accessed 9 May 2023.